

Document downloaded from:

<http://hdl.handle.net/10251/166968>

This paper must be cited as:

García Martínez, A.; Carlucci, P.; Monsalve-Serrano, J.; Valletta, A.; Martínez-Boggio, SD. (2020). Energy management strategies comparison for a parallel full hybrid electric vehicle using Reactivity Controlled Compression Ignition combustion. *Applied Energy*. 272:1-18. <https://doi.org/10.1016/j.apenergy.2020.115191>



The final publication is available at

<https://doi.org/10.1016/j.apenergy.2020.115191>

Copyright Elsevier

Additional Information

Energy Management Strategies comparison for a Parallel Full Hybrid Electric Vehicle using Reactivity Controlled Compression Ignition Combustion

Antonio García^{*},^a, Paolo Carlucci^b, Javier Monsalve-Serrano^a, Andrea Valletta^b and Santiago Martínez-Boggio^a

^a CMT - Motores Térmicos, Universitat Politècnica de València, Camino de Vera s/n, 46022 Valencia, Spain

^b Università del Salento, Piazza Tancredi, 7, 73100 Lecce, Italy

Applied Energy, Volume 272, 15 August 2020, 115191
<https://doi.org/10.1016/j.apenergy.2020.115191>

Corresponding author (*):

Dr. Antonio Garcia Martinez (angarma8@mot.upv.es)

Phone: +34 963876559

Fax: +34 963876559

Abstract

Reactivity Controlled Compression Ignition combustion technology potentials are well known for the capability to drastically reduce the engine-out nitrogen oxides and soot emissions simultaneously. Its implementation in mid-term low-duty diesel engines can be beneficial to meet the upcoming regulations. To explore the potential of this solution, experimental data are used from a compression ignition 1.9L engine, which is operated under two combustion-modes: Reactivity Controlled Compression Ignition and conventional diesel combustion. Meanwhile, also the carbon dioxide emissions limitations must be fulfilled. To achieve this goal, the benefits associated to powertrain electrification in terms of fuel economy, can be joined with the benefits of RCCI combustion. To do so, two different supervisory control strategies are compared: Adaptive Equivalent Minimization Control Strategy and Rule-Based Control strategy, while dynamic programming is used to size the electric grid of the powertrain to provide the best optimal solution in terms of fuel economy and emissions abatement. The analysis of the designed hybrid powertrain is carried out numerically with GT-Suite and Matlab-Simulink software. The results show a great potential of the parallel full-hybrid electric vehicle powertrain equipped with the dual-mode engine to reduce the engine-out emissions, also to increase fuel economy with respect to the homologation fuel consumption of the baseline vehicle. The optimal supervisory control strategy was found to be the emissions-oriented Adaptive Equivalent Minimization Control Strategy, which scores a simultaneous reduction of 12% in fuel consumption, 75% in engine-out nitrogen oxides emissions and 82% in engine-out soot, with respect to the baseline conventional diesel combustion engine vehicle.

Keywords

RCCI, Energy Management, ECMS, Hybrid powertrain, Emissions regulations

1. Introduction

The year 2020 is marked by the enforcement of new emission regulations in the European Union, concerning the carbon dioxide (CO₂) emissions: for the passenger vehicles sector this means a 27% reduction compared to the previous regulation [1]. On the other hand, also noxious emissions, such as nitrogen oxides (NO_x) and soot, which are currently regulated by the Euro 6 regulation [2], are expected to undergo a severe reduction limitation in the upcoming years. In this sense, the benefits of diesel engine in terms of fuel economy are renowned, however the recent “diesel-gate” scandal has overshadowed this technology and harmed its employment for road transport. Also, the high costs of the aftertreatment systems with which a diesel vehicle is equipped, do not make the hybridization of diesel powertrain cost competitive, as compared to hybrid gasoline powertrains. Meanwhile, the electrified vehicles are becoming more available in the market since almost all major car manufacturers provide electrified solutions in their car fleet, even though support by governments to address financial barriers which prevent their market penetration are still required [3]. The sustainability of fully electrified transportation scenario is still a point of great discussion and concern, for instance when adopting a well-to-wheel analysis, the environmental impact of electric vehicles may result higher than for conventional vehicles, which also depends on the electric energy production mix of a country [4,5]. For this reason, in the following years, the electric hybrid vehicles will be the bridging technology towards the zero-emissions transportation, so it is expected that the combustion engine will still play a determinant role in the road transport.

Novel combustion technologies and the employment of alternative fuels with lower carbon footprint would be crucial to meet the upcoming stringent targets. In this sense a transportation mix may be considered the best midterm solution, and a specific engine architecture should not be demonized a-priori [6]. Reactivity Controlled Compression Ignition (RCCI) is a dual-fuel technology that uses two fuels with different reactivity to promote a low-temperature combustion (LTC), simultaneously achieving very low NO_x and soot emissions. This technology can make the compression ignition (diesel) engine very competitive in terms of engine-out noxious emissions abatement with respect to the conventional diesel combustion (CDC) [7], and it has been analyzed for different engine platforms as well as for different fuels combinations [8,9]. At a counterpart, the RCCI combustion results in high carbon monoxide (CO) production and total hydrocarbons (THC) formation, and although part of the aftertreatment system (ATS) could be downsized due to the very low engine-out NO_x and soot emissions, it would still require an efficient diesel oxidation catalyst (DOC) converter, also considering the low operating temperatures of RCCI [10,11].

The benefits of implementing this combustion technology onboard of an electrified powertrain was proven by Garcia et al. [12]. In particular, the case of a series hybrid vehicle concept equipped with a retrofitted diesel engine to operate in RCCI mode with ethanol-diesel fuels over the World-wide harmonized Light-duty Test Cycle (WLTC) and Real Driving Emission cycle (RDE) driving cycles was studied [13]. The results show an

average reduction for the engine-out NO_x, soot and CO₂ of 90%, 98% and 10% respectively, thus satisfying the Euro 6 regulation. However, the cost of a series hybrid powertrain (distinct generator and motor units must be provided) makes it less competitive than the more widespread solution of parallel hybrid architecture, furthermore the parallel architecture can achieve good drivability and fuel economy compared to more complex solutions such as the power-split and the multi-mode architectures [14]. In the work of Benajes et al. [15], study with the diesel-gasoline RCCI engine was performed for both the parallel and mild hybrid architectures. In particular, numerical analysis was performed by implementing a supervisory controller for the powertrain energy management built with Rule-Based Control (RBC), which requires great calibration effort. Parallel hybrid vehicles integrate a supervisory energy management control unit, which has the key task to best split the power request between the internal combustion engine (ICE) and the electric machine (EM) while operating with a charge sustaining mode, which means that the battery energy content must be preserved. For more than two decades, different control strategies have been investigated for this purpose. Rule-based control strategies, also called heuristic strategies, are an ensemble of ad-hoc rules which define the operational status of the ICE and the EM for each operative case of the vehicle, according to some control parameters as, for instance, the vehicle speed and the rechargeable energy storage system (RESS) state: complex design of these kind of strategies is able to provide very good results in terms of fuel economy, when compared to the benchmark solutions obtained with dynamic programming (DP) [16]. On the other hand, optimal control strategies are based on an optimization problem, where the cost function (either objective function) may be for example the fuel consumption of the vehicle. It is of great interest the approach made with Equivalent Minimization Control Strategy (ECMS) that tries to assess the minimization of the consumption cost problem on-line, which means that the representative optimization problem is solved in real-time [17]. Recent upgrades of this algorithm have provided predictive-like features to improve its performance, for instance by harnessing data for future driving conditions based on traffic [18–20]. Furthermore, more sophisticated approaches, which use model prediction techniques, have been investigated to provide better predictability of the driving cycle characteristics so to improve the optimization of the fuel consumption [21–23]. However, these control strategies are not of easy implementation as they must rely on accurate powertrain dynamics modelling.

In the present work, the authors present a thorough investigation on the effect of different control strategies for the supervisory energy management control of a P2 parallel full hybrid electric vehicle (FHEV) equipped with a dual-mode engine the innovative contribution is the development of an ECMS based supervisory control strategy, oriented to NO_x emissions reduction, to specifically operate the engine that integrates RCCI combustion. Moreover, an exhaustive comparison between this strategy and the RBC one is made to highlight the main potentials. The results also proves that parallel architecture topology can be still a good choice to simultaneously reduce vehicle emissions and fuel consumption, without the need to increase the complexity of the

hybrid powertrain to enable the use of the compression ignition engine as in the cases previously mentioned of the series hybrid vehicle or in the solution proposed by Finesso et al. [24]. The same engine used in the work of Garcia et al. [12], was adopted. Furthermore, in the scientific literature there can be found research studies which make use of either design of experiment analysis or optimization tools to determine the best sizes of the hybrid powertrain electric hardware [25–27], while in this work the electrification of the powertrain is analyzed through DP optimization algorithm to assess the best sizing of the electric grid in terms of battery capacity and electric machine power. The energy management supervisory control was setup with both RBC and adaptive Equivalent Consumption Minimization Strategy (a-ECMS) strategies. The use of the latter, is encouraged by the works of Musardo et al. [28] and Nüesch et al. [29]: in the former, it is investigated the case study of a hybrid vehicle equipped with a dual-mode combustion engine running with Homogeneous Charge Compression Ignition Combustion technology (HCCI) and CDC; the latter analyses the efficacy of implementing into ECMS control strategy, a penalty to control NOx emissions produced by a diesel hybrid electric vehicle over a driving cycle. The comparison between these two types of supervisory control strategies is made on two bases: fuel consumption and NOx emissions reduction. The true potential of the powertrain under study was determined for both fuel-economy and emissions-oriented calibrations, through the analysis with DP which finally serves as a benchmark to compare the results given by a-ECMS and RBC control strategies. To investigate the vehicle behavior in the current homologation legislation, the WLTC driving cycle is considered.

2. Materials and Methods

2.1 Experimental test bench for RCCI combustion

The experimental campaign for this work was performed in a single-cylinder engine with the same characteristics of a commercial GM 1.9L four-cylinder turbo engine. The commercial ICE was calibrated by the original equipment manufacturer (OEM) to achieve Euro 4 legislation. The authors performed a re-calibration by injecting gasoline via the port fuel injection (PFI) and by injecting diesel (the high reactivity fuel) via direct injection (DI), using the original diesel fuel line. This allows to operate the engine under RCCI mode with two fuels injected in separated lines. For comparison, the whole calibration in CDC mode was repeated to validate the test bench. Table 1 summarizes the most relevant characteristics of the engine. More details of the test bed configuration and characteristics can be found in previous works [30,31].

Table 1 – Single cylinder GM engine characteristics.

Engine Type		4 stroke, 4 valves, direct injection
Number of cylinders	[-]	1
Displaced volume	[cm ³]	477
Stroke	[mm]	90.4
Bore	[mm]	82
Piston bowl geometry	[-]	Re-entrant
Compression ratio	[-]	17.1:1
Rated power @ 4000 rpm	[kW]	27.5
Rated torque@ 2000-2750 rpm	[Nm]	80

The main constraints that restrict the use of RCCI over the entire map are the mechanical limitations of the ICE and the elevated THC and CO emissions. In fact, at high loads, the excessive pressure rises rates (PRR), due to the autoignition of the gasoline in the compression stroke, limit the RCCI operation. This problem could be solved by increasing the recirculated exhaust gases (EGR) rates, but the OEM air management system limited this ratio to 50%. At low loads, the CO and THC are too high due to low temperature during the combustion event. Therefore, the engine thermal efficiency suffers an important drop. Lastly, at high engine speeds it is not possible to work with a single-cylinder engine due to mechanical limitations. A dual-mode operation map was generated combining the RCCI and CDC results, as shown in Figure 1a. The black points show the new calibration with RCCI mode and white points represents the measured CDC points. The RCCI region, due to the narrow range achieved, was discretized in 24 operative points. On the other hand, 76 operative points were measured for CDC.

As can be inferred from Figure 1a, the fuel consumption slightly increases under RCCI operation mode (25 g/kWh) because of the lower flame propagation. The restriction in maximum PRR does not allow to retard the diesel injection, resulting in a small loss in brake thermal efficiency (BTE). The main advantage of RCCI is the possibility to achieve low temperature combustion operation by adding high EGR rates together with a premix combustion operation. Figure 2 shows the gasoline fraction (low reactivity fuel) and the EGR rate for the dual-mode combustion strategy. The gasoline fraction (GF) was tuned between 49%-86%, with an average value around 69% for the RCCI operative points, as represented in Figure 2a. For the CDC combustion, the OEM used up to 30% of EGR. It is interesting to note that the EGR is used in a zone like the one selected to perform the RCCI mode. This is mainly because the Euro 4 regulation relied on the New European Driving Cycle (NEDC) driving cycle. On the other hand, in order to achieve the LTC mode, it is necessary to employ higher EGR rates. For this calibration, EGR rates in the range of 36%-44% were used, with average of 40%, as shown in Figure 2b.

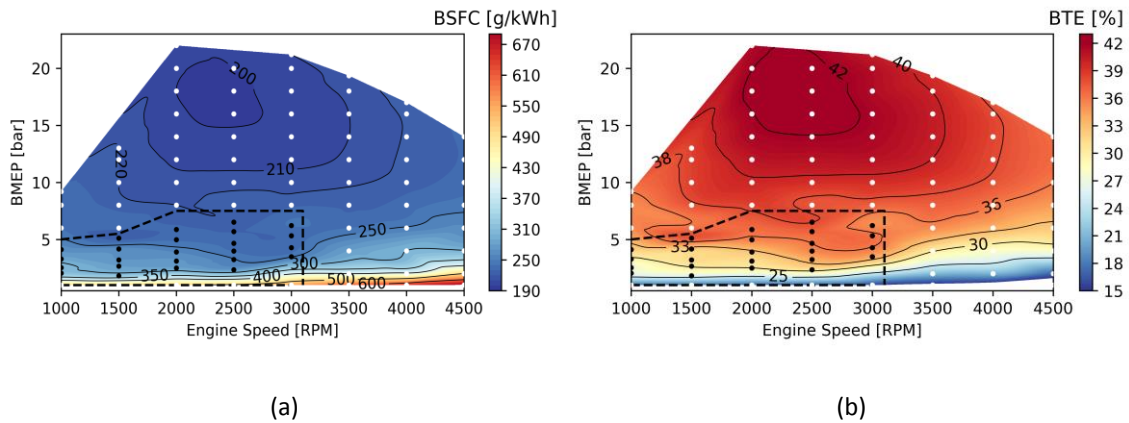


Figure 1 – Brake specific fuel consumption (a) and brake thermal efficiency (b) for the dual-mode calibration concept.

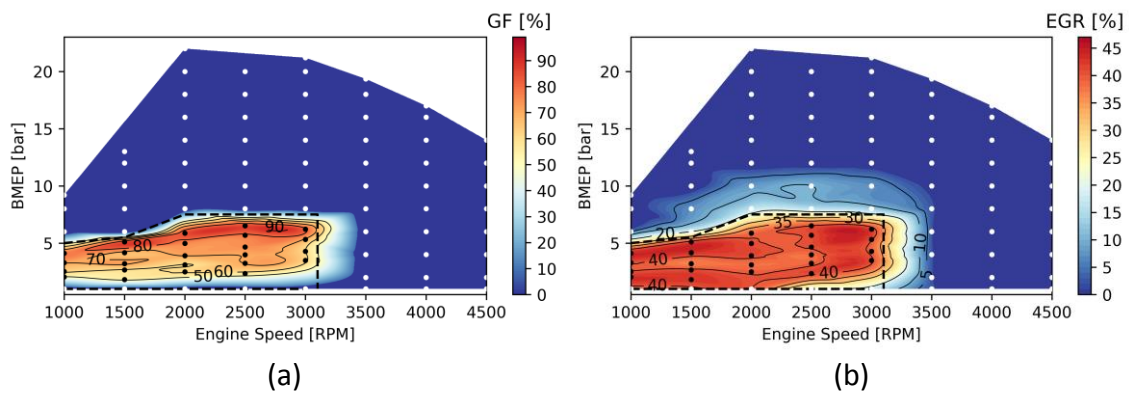


Figure 2 – Gasoline fraction (GF) (a) and exhaust gas recirculation (EGR) rate (b) for the dual-mode calibration concept.

The use of a low reactivity fuel and high EGR rates allows to achieve ultra-low NO_x and soot emissions. Figure 3a shows the NO_x emissions at stationary conditions for both combustion modes. In the case of RCCI, the NO_x level was below 0.46 g/kWh with a minimum of 0.10 g/kWh. Figure 3b shows the soot emissions for the dual-mode combustion. The advantage of coupling both modes in terms of soot emissions is larger than for NO_x. The CDC at high loads is characterized by ultra-low soot values (below 0.05 g/kWh), as with RCCI at low loads. For the case of RCCI, the average soot emission was 0.002 g/kWh.

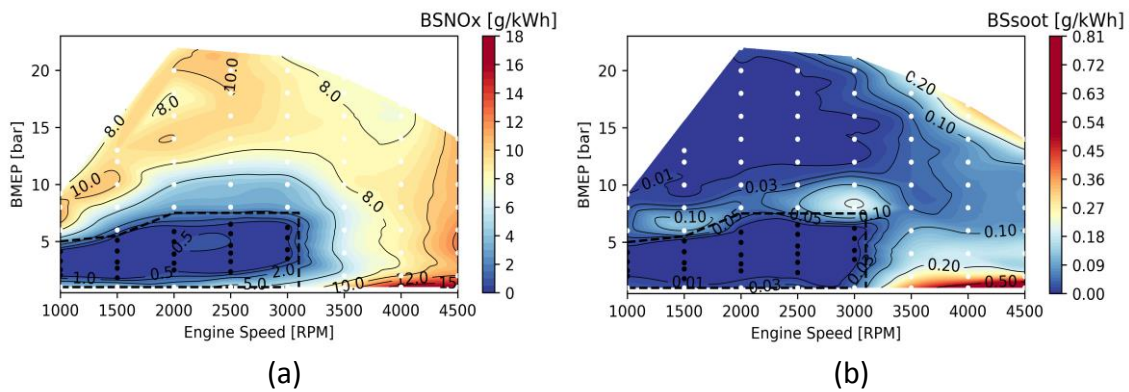


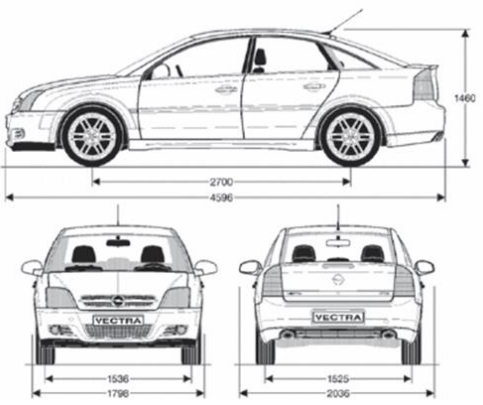
Figure 3 – Brake specific NO_x emissions (a) and brake specific soot emissions (b) for the dual-mode calibration concept.

2.2 Full electric hybrid P2 vehicle model

The vehicle model developed for this study uses the technical specifications of the original OEM platform equipped with a CDC engine. The main characteristics of the baseline vehicle are reported in Table 2.

Table 2 – OEM vehicle original platform.

Vehicle Technical Specification		
Vehicle Type		OEM
Base Vehicle Mass [kg]	[kg]	1523
Passenger and Cargo Mass	[kg]	100
Fuel Mass	[kg]	45
Vehicle Drag Coefficient	[-]	0.28
Frontal Area	[m ²]	2.04
Tires Size	[mm/%/inch]	225/45/R118
Differential Ratio	[-]	3.2
6 Speed Transmission ratios (1,...,6)	[-]	3.82, 2.05, 1.3, 0.96, 0.74, 0.61



P2 parallel full hybrid powertrain (FHEV) architecture (Figure 4), differs from the conventional platform due to the presence of: the EM, which can operate both as a generator and as a motor; a high voltage battery pack (HV Batt) and its associated electric grid made of inverter, DC/DC converter; one additional clutch (K0), through which the internal combustion engine can be decoupled at convenience, in order not to have the drag losses whenever the vehicle is only propelled by the electric machine. The transmission (TRN) may remain the same as the one present in the conventional vehicle. The interdependence between the powertrain components is clear as well as their influence on the powertrain performance for a given driving cycle.

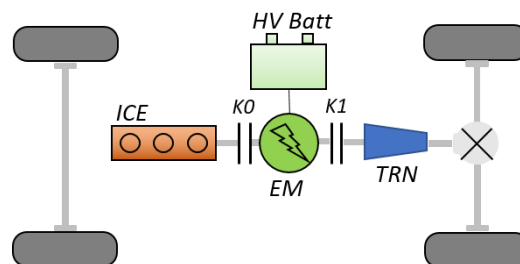


Figure 4 – Parallel P2 FHEV powertrain architecture

Therefore, in the present study, a design methodology, based on the Dynamic Programming (DP) algorithm, was adopted in order to size the main powertrain components that have the greatest impact on the energy management problem: these are the electric machine power and the battery capacity. The analysis was finally performed for different gearshift schedules (later explained) which determine the operational speed of both ICE and EM. The advantage of using DP is that it can provide a global optimal solution in terms of energy management with respect to a defined cost function (e.g. fuel consumption, noxious emissions cost or a combination of the two);

hence it is possible to determine the best hardware for the given powertrain by sweeping several combinations of the above cited design components.

Regarding the gearshift schedule, for the six speed transmission gearbox (same than the OEM), it was assumed that upshift is operated at a determined rotational speed, which would be a fraction of the maximum engine rotational speed, according to the value of a “gearshift coefficient”. For different values of gearshift coefficient, different gearshift schedules can be thus derived: downshift schedule is suitably derived starting from the upshift in order to prevent gears selection toggling.

The transient behavior of the ICE, EM and the battery has been carried out through numerical modelling by means of GT-Suite software, making use of experimental data. For this purpose, the engine and the electric machine are modelled following the steady-state map-based approach. Although the authors are aware that the map-based approach does not allow an accurate modelling of the transient behavior of the ICE, possibly leading to an underestimation of the real engine-out emissions, the choice of this method is dictated by its lower computational cost with respect to dedicated dynamic models. In fact, the latter ones would require an accurate model of the air path together with a predictive model of the combustion process in order to realistically estimate the ICE behavior, but the computational time would be two order of magnitude higher than for a map-based approach in case a full-scale 1D-CFD is implemented [32]. Furthermore, as presented in a previous work of the research group [33], the deviation in terms of emissions is below 5%. Consequently, this method is more suitable for the goal of the present work which is to study the effect of high-level control strategies on overall fuel consumption and engine-out emissions. The maps for fuel consumption and engine-out emissions considered for the present work were presented in Figure 1 and Figure 3.

The electric machine efficiency map was taken from the GT-Suite library and it is reported in Figure 5. Later, it was properly rescaled, given the characteristics – torque range of (-400Nm, 400Nm) and maximum rotational speed of 6000rpm – of the original map. In particular, the maximum speed range was reduced by a scale factor of 0.8, so to match the maximum rotational speed of the ICE: this can be justified by the fact that in a P2 FHEV, the electric machine rotational speed is linked to that of the engine. Power scaling was done through a multiplier coefficient for the torque output, which hence is the other powertrain design parameter, equally applied to both generator and motor parts of the original map [34]. Finally, the EM weight is estimated assuming a gravimetric power density of 1.6 kW/kg [35].

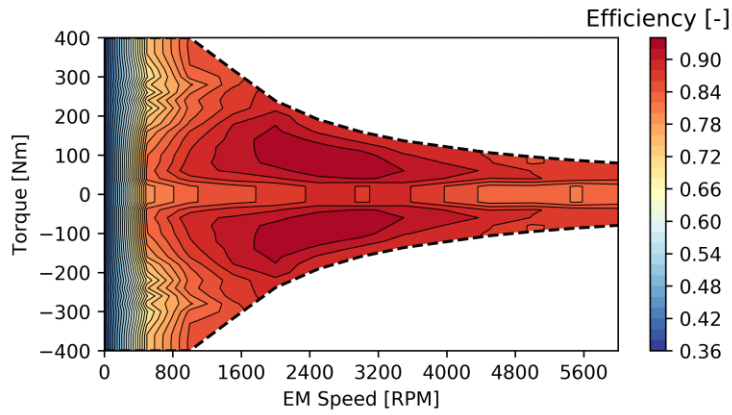


Figure 5 – Electric machine efficiency map

The vehicle Rechargeable Electric Energy Storage System (REESS) is modelled as a Li-Ion battery pack. Due to the lack of in-house experimental data concerning the characterization of battery cells, data available from a literature review for LiFePO₄ cell was used [36,37]. In particular, the use of this type of cell technology is encouraged by the maturity of its application in the automotive field as well as by its reliability in terms of safety issues when compared to higher energy density lithium-cells [38]. The battery electrical circuit model is built starting from the cell model. The equivalent electrical circuit model used for the cell is a Thévenin circuit with two parallel resistor-capacitor sub-circuits. With respect to the simple internal resistance model, it provides better modelling of the cell electrical dynamics: i.e. diffusion processes, even though it does not consider hysteresis effects, which were not modelled due to the lack of data. The dependence on temperature and state of charge (SoC) of all the resistances and capacitors present in the model, both for discharge and charge operations, is formulated according to the work by Perez et al [37], where the electro-thermal model for 26650 LiFePO₄ cell (manufactured by A123 Systems) is validated against voltage and cell surface temperature measurements from real driving cycles experiments. The final battery characteristics are derived by knowing the number of parallel cells, which must satisfy the design capacity which results from the preliminary design study with DP, and the number of series cells, which must satisfy the nominal voltage constraint of the powertrain electric grid design. The choice of the voltage level fell on 400V, which is a typical figure for high voltage FHEVs. The battery electrical characteristics are reported in Table 3.

Table 3 – Li-Ion battery main specifications

Cell Technology	LiFePO ₄ (manufactured by A123 Systems)	
Cell Open Circuit Voltage	[V]	3.3
Cell Capacity	[Ah]	2.3
Cell weight	[kg]	0.076
Battery Open Circuit Voltage	[V]	400
Battery Design Capacity	[Ah]	10
Number of Series cells	[-]	122
Number of Parallel cells	[-]	3

Regenerative braking control is a characteristic feature of the hybrid powertrains and enables the vehicle kinetic energy recuperation during the braking phases, which would otherwise be dissipated by conventional mechanical friction brakes. Referring to the P2 PHEV hybrid architecture, considering that the electric machine is linked to the driving wheels through the transmission-differential, only the braking power requested at the driving wheels can be potentially recuperated. Moreover, due to mechanical inefficiencies, as well as electrical inefficiencies (electric machine and inverter), only part of the available kinetic energy during braking events can be recuperated and stored in the REESS. In fact, considering the inefficiency of the mechanical-to-electric energy conversion process, energy recuperation through regenerative braking is not always beneficial, especially at very low speeds [39]: generally, a reference value of minimum speed above which regenerative braking can be activated is 5-8 km/h. When considering a braking event, it is mandatory to always fulfill stability requirements: for example, according to European braking legislation, since the vehicle modelled belongs to vehicle class M1, it has to fulfil the Braking regulation ECE13-H [40]. According to the classification of the cited regulation, the electric regenerative braking system of category B is considered, hence it is part of the vehicle braking service system. Concerning stability, the braking power demand might be conveniently split between the front and rear axles. Therefore, it implies that only part of the vehicle kinetic energy can be potentially recuperated during a braking event. Furthermore, additional limits may reduce the amount of regenerative braking recuperated energy, which are the operative maximum torque limit of the electric machine and the power limit set by the battery: the limitations on the maximum charging power are related to the maximum state of charge and the maximum charge current. All these issues should be considered when modeling a given hybrid powertrain, in order not to overestimate energy recovery which would lead to too optimistic results in terms of fuel economy, for a given driving cycle. In the present work, the braking power request distribution has been split between the front and rear axles according to stability constraints. The ideal braking distribution ensures that front and rear wheels lock simultaneously, which was derived according to equation (1):

$$\begin{aligned} F_{front\ axle}^{ideal} &= \dot{v} \frac{m}{L} \left(L_R + m \frac{\dot{v}}{g} h_f \right) \\ F_{rear\ axle}^{ideal} &= \dot{v} \frac{m}{L} \left(L_f - m \frac{\dot{v}}{g} h_f \right) \end{aligned} \quad (1)$$

Where \dot{v} is the vehicle longitudinal acceleration, m the vehicle mass, L the wheelbase length, L_R and L_f respectively are the distances of the rear and front axles from longitudinal position of the center of gravity and h_f is the height of the center of gravity (this is estimated to be 30% of the vehicle height). The effect of the regenerative braking control model on kinetic energy recuperation can be concretely quantified for the vehicle under study over the WLTC driving cycle: the total kinetic energy available during vehicle braking phases is 1.04 kWh and the recuperated energy, that is the kinetic energy converted into electric energy by the EM, is equal to 0.56 kWh.

Prior to the discussion about the supervisory control strategies developed for the hybrid powertrain, it is important to clarify its characteristics and hence the operational degrees of freedom. The hybrid powertrain architecture topology characterizes the

operating modes through which the power demand is split between EM and ICE. In a P2 parallel hybrid architecture (Figure 4), the presence of two clutches (K0 and K1) enables: the disengagement of the ICE to reduce drag losses whenever the electric machine is used for traction; to increase the potential recuperative energy during the braking phases. The possible operating modes for a P2 parallel architecture, both in case of both positive and negative power requests, are depicted in Figure 6 and they are here briefly summarized:

- E-drive mode – vehicle propulsion is performed only with the EM
- ICE-drive – vehicle propulsion is performed only with the ICE
- E-boost – vehicle propulsion is mainly performed by the ICE which is assisted by the EM to satisfy peak power demands
- Load Point Shifting (LPS) – vehicle propulsion is performed by ICE, which provides extra power so to recharge the battery (EM operates in generator mode)
- Regenerative Braking – considering the braking power required at the driven axle, EM provides the maximum braking power, which recharges the battery
- Parallel Braking – considering the braking power required at the driven axle, the braking power is split between friction brakes and electric machine.

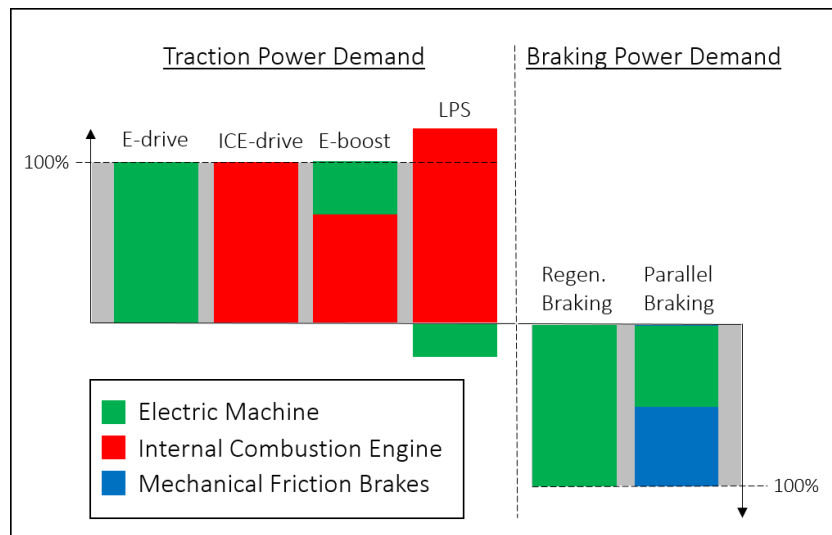


Figure 6 – Schematic bar chart showing P2 FHEV operating modes and power shares between EM and ICE during traction, and EM and mechanical friction brakes during braking.

2.3. Vehicle components sizing with dynamic programming

The sizing approach used in this work is to run a design of experiment (DoE) analysis with DP: the powertrain design factors are optimized over the WLTC driving cycle. Thanks to this preliminary analysis, the best set of electric machine size and battery capacity, can be identified and later be used to run the analysis on the actual vehicle model incorporating the on-line energy management strategies. Two different design analysis are carried out based on two different objectives: the first one is to identify the best configuration of design parameters for a fuel-economy-oriented optimization, the second one aims to understand how an emissions-oriented optimization would affect the prior result.

The DP algorithm is based on the Bellman principle of optimality and it has been extensively used in literature to optimize control problems to find the global optimum solution of a given cost function, in terms of state and control trajectories over a known time horizon. The DP numerical algorithm used for the present analysis was developed by Olle Sundström and Lino Guzzella [41]. A 0-D vehicle model was hence developed with Matlab, which is used by the DP algorithm: the vehicle model includes an equivalent internal resistance model for the battery, a regenerative braking control strategy model (equal to the one adopted for the simulations of the full-vehicle model incorporating the on-line control strategies). Also, the data concerning all the components of the powertrain (ICE, EM, battery cell, transmission, chassis) maintain the same specifications. The cost function used for the fuel-economy oriented sizing problem, is the integral of the fuel consumption over the driving cycle, expresses in equation (2):

$$J(u(t)) = \int_0^{t_f} \dot{m}_{fuel}(u(t), t) dt \quad (2)$$

where \dot{m}_{fuel} is the fuel mass flow rate and $u(t) = T_{EM}/T_{ICE}$ is the control variable of the problem at time t , which is represented by the torque split between the ICE and EM.

On the other hand, the case of NO_x-emissions oriented sizing is explored. The cost function implemented in the DP adds a penalty cost term, associated to the NO_x emissions \dot{m}_{NOx} , multiplied by a weight factor β , as written in equation (3):

$$J(u(t)) = \int_0^{t_f} [\dot{m}_{fuel}(u(t), t) + \beta \dot{m}_{NOx}(u(t), t)] dt \quad (3)$$

A full factorial DoE was run on a wide design parameters domain with 3200 treatments and 3 factors, which are reported in equation (4) with the respective sets of levels values:

$$\begin{cases} \text{Battery Capacity} \in [2, 15] Ah \\ \text{Electric Machine scale factor} \in [0.2, 1] \\ \text{Gearshift coefficient} \in [0.33, 1] \end{cases} \quad (4)$$

the minimum value for the gearshift coefficient corresponds to a maximum engine upshift speed of 1500rpm. For the sake of clarity, the battery and EM weights were adjusted for each case, following the procedure explained in section 2.2.

2.4. On-line energy management strategies

The on-line control strategies, the a-ECMS and RBC, were designed and implemented in a Matlab-Simulink code, which was then paired to the vehicle model developed in GT-Suite. Therefore, the control strategy was fully developed separately from the GT-Suite powertrain model: the control signals output by the on-line supervisory energy management control (built in Simulink) are sent to the powertrain model (built in GT-Suite) to control the internal combustion engine, the electric machine and the actuation of the clutches, as shown in the schematic representation in Figure 7. This methodology

allows to use a more sophisticated control strategy while maintaining the benefits of keeping the well-known GT-Suite powertrain modelling software architecture.

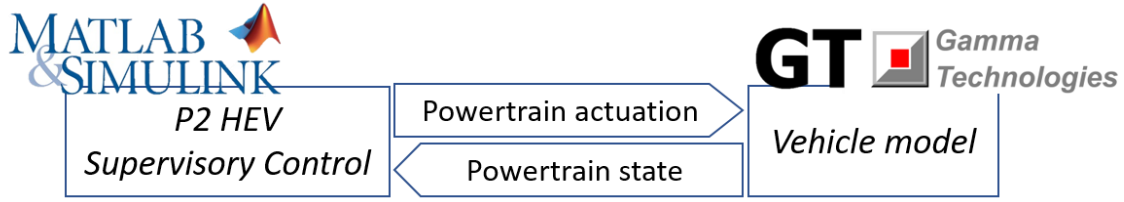


Figure 7 – Schematic representation showing the coupling between the supervisory energy management control built in Matlab-Simulink and the vehicle model built in GT-Suite.

2.4.1. Rule-Based Control strategy

The rule-based control strategy has been previously developed and discussed by Benajes et al [15,33]. Ad-hoc rules are adopted to operate the P2 FHEV powertrain for all the possible operating modes as already discussed. The control strategy characteristics are schematized in Table 4 for clarity. In general the operating modes are selected according to the driver desired torque T_{driver} and the value of battery SoC, while ensuring that the power units mechanical limits ($T_{ICE,max}$, $T_{ELM-mot,max}$, $T_{ELM-gen,max}$) are satisfied. The EM is set to operate in generator mode to charge the battery and its torque output value is determined by a PID controller (to be calibrated) that acts on the signal ($SoC - SoC_{target}$). Also, the control parameter $v_{lim,EV}$, to be calibrated, is set to decide the speed up to which the vehicle can run in full electric mode. During the power assist mode, the power split between the ICE and EM is set by the control parameter $Split_{coef}$, which must be tuned.

Table 4 – Conditions for each operative mode of the RBC supervisory controller – EV is full electric vehicle operation.

Vehicle State	Sub-State	Conditions		ICE	EM
EV	EV traction	$T_{driver} > 0$ & $0 < v_{veh}$ < $v_{lim,EV}$	$Charge_{state} = 0$	$T_{ICE} = 0$	$T_{EM} = T_{driver}$
HEV – Traction	ICE Start	$T_{driver} > 0$ & $v_{veh} > v_{lim,EV}$	$n_{ICE} < 1000$	$T_{ICE} = 0$	$T_{EM} = T_{driver} + T_{ICE\ start}$
	Charging		$Charge_{state} = 1$	$T_{ICE} = T_{driver} + T_{charge}$	$T_{EM} = -T_{charge}$
	Power Assist		$Charge_{state} = 0$ & $Split_{coef} * T_{driver} < T_{EMmax}$	$T_{ICE} = (1 - Split_{coef}) * T_{driver}$	$T_{EM} = Split_{coef} * T_{driver}$
	Power Assist Max ICE (EM boost)		$T_{driver} > T_{ICE,max}$ & $SoC > SoC_{min}$	$T_{ICE} = T_{ICEmax}$	$T_{EM} = T_{driver} - T_{ICEmax}$
HEV – Braking	Regenerative Braking	$T_{driver} < 0$ & $v_{veh} > 0$	$SoC < SoC_{max}$ & $T_{driver} > T_{EMmin}$	$T_{ICE} = 0$	$T_{EM} = T_{driver}$
	Parallel Braking		$SoC < SoC_{max}$ & $T_{driver} < T_{EMmin}$	$T_{ICE} = 0$	$T_{EM} = T_{min}$
	Mechanical Friction Braking		$SoC \geq SoC_{max}$ or $v_{veh} < 5km/h$	$T_{ICE} = 0$	$T_{EM} = 0$

v_{veh} = vehicle speed; $v_{lim,EV}$ = vehicle speed limit for full electric operation; T_{driver} = driver desired torque; $Brake_{position}$ = 0% when brake pedal is no pressed, 100% when fully pressed; $Charge_{state}$ = control state variable equal to 1 when $SoC < SoC_{charge}$, equal to 0 when $SoC \geq SoC_{target}$; T_{EMmax} and T_{EMmin} are the maximum and

minimum EM torque output respectively in motor and generator modes; n_{ICE} is the rotational speed of ICE; $T_{ICE,max}$ is the maximum torque output of ICE.

Due to the number of parameters to be simultaneously optimized and to the large range that needs to be tested, a Latin Hypercube DoE was run with 800 cases:

$$\left\{ \begin{array}{l} Split_{coef} \in [0, 100]\% \\ v_{lim,EV} \in [5, 120] \text{ km/h} \\ Gearshift \text{ scale coefficient} \in [0.33, 1.00] \\ SoC_{charge} \in [0.40, 0.58] \\ SoC_{@Power_{charge \ max}} \in [0.40, 0.58] \end{array} \right. \quad (4)$$

Where SoC_{charge} is the value that triggers the battery charging and $SoC_{@Power_{charge \ max}}$ is a parameter used in the PID battery SoC controller to set the maximum battery charge power. This means that when the actual SoC reaches the value set by the above-mentioned parameter, the ICE will deliver the maximum available power (at the current ICE speed) to charge the battery. The lower the $SoC_{@Power_{charge \ max}}$ used, the softer the battery charging strategy is.

2.4.2. Adaptive Equivalent Consumption Minimization Strategy

Equivalent Minimization Control Strategy, originally developed by Paganelli et al. [17], is an on-line control strategy which has been widely developed over the past two decades and has proven to be very flexible to control the power distribution between the ICE and EM in hybrid vehicles. Differently from the DP and Pontryagin Minimum Principle (PMP) based control algorithms, the main advantage of the ECMS is that it can be implemented in a real vehicle engine control unit (ECU), while still being an optimal control based strategy, since it can instantaneously solve the power distribution problem without a-priori knowledge of the entire time horizon of the driving cycle. In fact, this control strategy would not provide an optimal solution, but a suboptimal one.

The ECMS introduces an instantaneous optimization problem, where the representative cost function is minimized at each time step. The performance of the ECMS control strategy then depends on how well it is calibrated, and also on the integration of possible upgrades of the algorithm, which enable feedback adaptation of the control parameters with respect to some powertrain state parameters over time. The cost function, used in the present work, to solve the optimization problem can be expressed as in equation (6):

$$H(SoC, \vec{u}(t), t) = Q_{LHV} \dot{m}_f(\vec{u}(t), t) + s(SoC, t) P_{batt}(\vec{u}(t), t) + p_1(NOx(t)) + p_2(\Delta T_{ICE}(t)) \quad (6)$$

where $u(t)$ is the control variable and it stands for the split between ICE and EM (similar effect of the $Split_{coef}$ in the RBC). $s(t)$ is the equivalence factor which allows to couple the electrical energy consumption together with the fuel consumption: it accounts for the chain of inefficiencies to convert energy from the fuel tank to the battery. In terms of minimization, the higher $s(t)$ the less convenient is to use the electrical energy, while the lower $s(t)$ the more convenient it is to use electrical energy to propel the vehicle. In literature, starting from Paganelli work, there are several methods used to define

$s(t)$: in very early works it is defined as a constant, which may change its value according to whether the battery is being discharged or charged. In more recent works, a feedback proportional integral formulation of $s(t)$ was developed and extensively used in order to provide a more suitable control for real-time applications: in particular the feedback control can be referred to the powertrain state variable of interest, the state of charge of the battery SoC . According to the work of Onori et al. [42], anytime a feedback control of some sort is integrated into the formulation of ECMS, so to enable self-adjustment of the control parameters during a driving cycle, the algorithm may be called “adaptive-ECMS” (a-ECMS). In the present work, a proportional feedback approach was chosen as it proved to enable faster and more responsive calibrations. The final formula for equivalence factor is then:

$$s(SoC, t) = s_0 \left(1 - \left(\frac{k_p (SoC(t) - SoC_{ref})}{\Delta SoC_{norm}/2} \right)^q \right) \quad (7)$$

Summarizing, a fuel-economy-oriented control strategy has the objective to minimize the fuel consumption. On the other hand, for an emissions-oriented control strategy, the objective would be also to minimize the specific emissions. Therefore, the integration of a-ECMS control strategy with RCCI technology requires an additional term into the cost function, $p_1(NOx(t))$, which penalizes the engine-out NOx . It is important to note that soot emissions were not specifically addressed in the present control strategy mainly because RCCI region ensures very low soot production as well as the CDC region at higher loads (see Figure 3b). As already discussed in section 2.1 and as shown in Figure 3a, the RCCI operational region for the employed engine is limited. For this reason, the supervisory control strategy should be able to promote the ICE to work in this region and suitably satisfy the torque demand with the aid of the electric machine.

Since the optimal split is selected out of a range/pool of power split candidates at each time-step, a different NOx emissions is associated to each of them, hence the idea is to apply a different penalty value according to the deviation of the NOx emissions for the i -th candidate, with respect to the minimum possible NOx emissions available in the candidates’ range, at each time-step. The penalty is further formulated with a piecewise function, represented in equation (8), in order to give a penalty value of zero to all the power split candidates, whose related engine torque output fell within the RCCI region.

$$p_1(NOx(t)) = \begin{cases} \beta \left(\frac{|NOx_{min} - NOx(u(t), t)|}{NOx_{max} - NOx_{min}} \right)^{2r} & \forall u(t) \text{ s. t. } T_{ICE}(t) \notin [T_{ICE,RCCI}^{min}, T_{ICE,RCCI}^{max}] \\ 0 & \forall u(t) \text{ s. t. } T_{ICE}(t) \in [T_{ICE,RCCI}^{min}, T_{ICE,RCCI}^{max}] \end{cases} \quad (8)$$

where β and r are two calibration parameters: in particular, the former is the penalty weight factor, the latter is the penalty order term.

In the present work, the ICE controls as well as EM controls are not specifically modelled, since it is out of the scope of this study: however, especially concerning the ICE, a smooth operational behavior must be ensured, also considering the typical “chattering” issues deriving from integration of the ECMS control strategy, as

commented by Serrao [43]. In fact, high ICE dynamics penalizes emissions, as proved by Grondin et al. [44], mainly at cold engine operation, and also impacts on drivability. For this reason, the last term in equation (9), $p_2(\Delta T_{ICE}(t))$, is designed to penalize high torque variations between consecutive time steps:

$$p_2(\Delta T_{ICE}(t)) = \gamma \left(\frac{\bar{T}_{ICE} - T_{ICE}^{act}}{\Delta T_{ICE}(n_{gear}(t))} \right)^{2t} \quad (9)$$

Where γ and t are calibration parameters, T_{ICE}^{act} is the current torque output of the ICE, while ΔT_{ICE} is the admissible ICE torque output variation which is calculated with respect to the engaged transmission gear, from an ad-hoc look-up table (Table 5):

Table 5 – Look-up table of allowed maximum ICE torque variation for the six-speed transmission

n_{gear}	1	2	3	4	5	6
ΔT_{ICE} [Nm/s]	50	40	40	35	30	15

This constrain was also considered in the RBC strategy for a valid comparison.

The a-ECMS supervisory control strategy was entirely developed in Matlab/Simulink, which was then coupled to the vehicle model built in Gt-Suite. Signals of vehicle state are passed to the Simulink vehicle supervisory control that manages the torque demand during both the traction and braking phases and hence also coordinates the engagement of the powertrain clutches K0 and K1.

3. Results and discussions

3.1. Dynamic programming sizing results

The results of the DoE analysis, performed with both the fuel-economy-oriented optimization and the emissions-oriented optimization, are shown in Figure 8 and Figure 9, respectively. For the sake of brevity, only the results for the most representative gearshift coefficients are reported, anyway it can be noticed how this parameter greatly affects the solution since it determines the regime of the ICE and EM. From Figure 8, it can be inferred that the fuel-economy-oriented optimization leads to a minimum fuel consumption of 4.14 L/100km at a gearshift coefficient of 0.44. To achieve this, a battery size of 6.9 Ah and an EM power of 20 kW are needed. It is interesting to remark that this value represents the global optimal solution in terms of fuel consumption that can be obtained with the current hybrid powertrain. For this reason, it can be used as benchmark configuration to evaluate the goodness of the on-line control strategies studied in subsection 3.2. Figure 8 also shows that the coefficient shift is the most crucial parameter to be selected in order to improve the fuel consumption. The battery capacity and EM power show a softer impact on the final fuel consumption results, in fact, for a fixed gearshift coefficient, the fuel consumption has a maximum variation of almost ± 0.2 L/100km with respect to the mean value.

Focusing on reducing NOx emissions (Figure 9), it can be seen that the emissions-oriented optimization minimum value for NOx emissions is equal to 0.047 g/km, which is below the current Euro 6 limit (0.08 g/km for CI ICE). Therefore, the required

powertrain configuration differs from the one obtained for fuel-economy-oriented optimization. In particular, the battery capacity increases from 6.9 Ah to 9.2 Ah, while the EM power from 20.0 kW to 36.5 kW. The increase of the EM power can be explained in two ways: first, it is due to the necessity of more flexibility to operate under pure electric and power assist modes to not use the higher load region of the ICE map, where the highest NOx emissions are generated (Figure 3a); second, it depends on the scaling procedure used for the EM map (explained in subsection 2.2) which expands the high efficiency region for higher EM powers, where operating points fall (Figure A1h).

To have more information about the vehicle components behavior, Figure A1, in the appendix A, shows the operative points and battery state of the charge for the optimum case for both DP strategies. The SoC trajectory in the emissions-oriented case is inverted compared to the one of the fuel-economy case (Figure A1a and A1b respectively) and this depends on the fact that as the ICE power is forced to operate in the RCCI region, the battery energy cannot be restored through LPS operating mode as in the fuel-economy case. Thus, the optimal energy use requires to recharge the battery in advance to later use it when the driving cycle requested power is higher. This can be also inferred by comparing the torque curves of ICE and EM for both cases (Figure A1c and A1d). Figure A1g and Figure A1h show the difference in terms of EM operation.

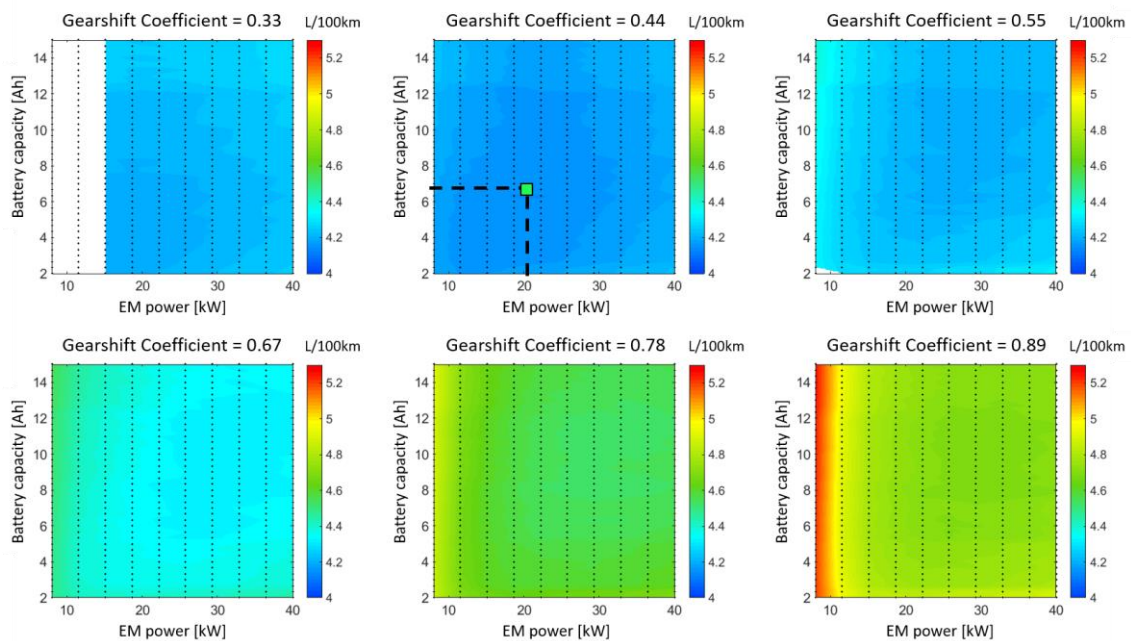


Figure 8 – Contour plots showing fuel-economy-oriented DP DoE analysis. The optimal fuel consumption, green square marker, achieves fuel consumption 4.14 L/100km with configuration {Battery capacity = 6.9 Ah, EM power = 20 kW, gearshift coefficient = 0.44}

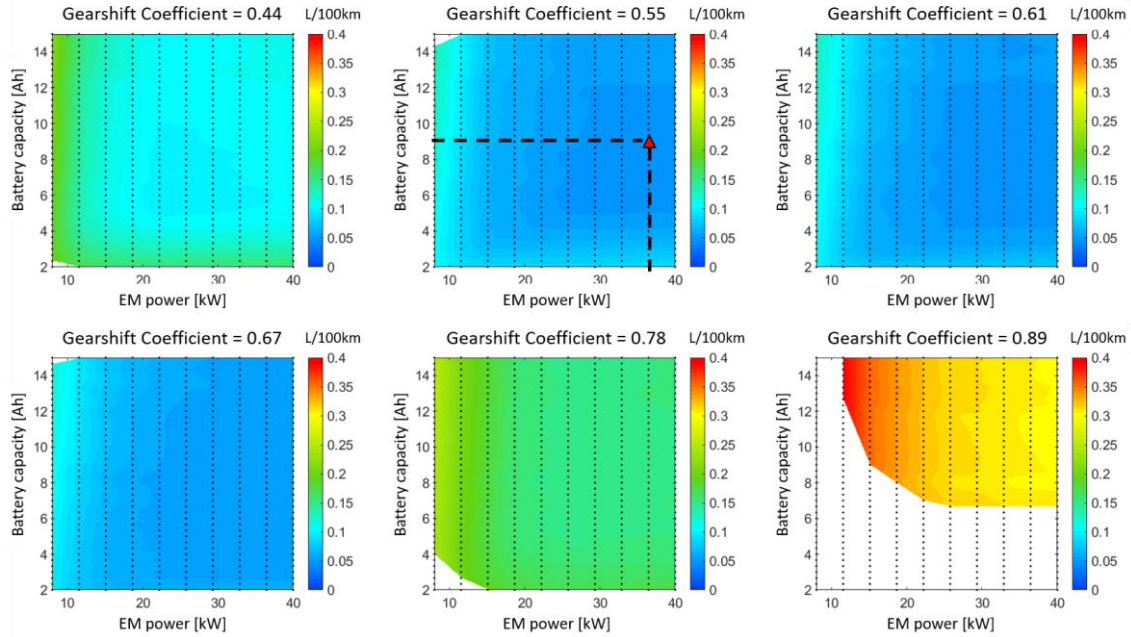


Figure 9 – Contour plots showing the NOx emissions-oriented DP DoE analysis. The lowest NOx emissions level is 0.047 g/km, red square marker, achieved with a configuration {Battery capacity = 8 Ah, EM power = 36.5 kW, gearshift coefficient = 0.55}. Unfeasible solutions are in blank.

In order to evaluate the on-line control strategies in subsection 3.2, one of the two configurations of battery capacity and EM power, previously described, must be selected. To do this, the optimal configuration for fuel-economy oriented DP has been tested with the best gearshift coefficient value found with the emissions-oriented strategy (0.55), and vice-versa. From Table 6, it can be seen that the configuration derived for fuel economy (with smaller battery and electric machine than emissions-oriented configuration) also manages to obtain NOx emissions below the Euro 6 limit, when the emissions-oriented DP is applied (0.057 g/km of NOx). For this reason, it will be selected as reference configuration. Nonetheless, it is interesting to note that this solution leads to a 14% fuel consumption penalty with respect to the global optimum (4.72 to 4.14 L/100km).

Table 6 – Evaluation of optimal DP solutions

	Fuel-economy-oriented DP		NOx emissions-oriented DP	
	FC [L/100km]	NOx [g/km]	FC [L/100km]	NOx [g/km]
Best fuel-economy configuration (6.9 Ah, 20.0 kW and GS 0.44)	4.14	1.36	4.72	0.057
Best emissions-oriented configuration (9.2 Ah, 36.5 kW and GS 0.55)	4.17	1.22	4.74	0.047

*Euro 6 NOx limits for CI is 0.080 g/km

3.2. RBC vs a-ECMS calibration

The best sizes of battery and EM (6.9 Ah and 20.0 kW respectively), obtained in subsection 3.1, are used in the vehicle model to compare the potential of the on-line control strategies for the WLTC driving cycle: RBC and a-ECMS. The calibration of the

two strategies was performed once again also considering different gearshift schedules: this can be explained by the fact that the gearshift schedule is strictly correlated to the control strategy and both online control strategies implement additional constraints, as the ICE torque derivative limiter, which was not included in the DP optimization. The general method adopted for the calibration of the on-line control strategies was to have a deviation of final SoC value from the reference value lower than $\pm 1\%$. In this way, a null net battery energy balance is guaranteed over the driving cycle and the comparison between the two on-line control strategies and as well with the DP results, is fair and will not require any energy correction to account for possible deviation between the final SoC achieved and the SoC target.

The calibration of the RBC supervisory control strategy is achieved through DoE analysis. The results of this methodology are represented in Figure 10, where the best solutions are identified in terms of minimum fuel consumption, for the case of fuel-economy oriented strategy, and in terms of minimum NOx emissions, for the case of emissions-oriented strategy. The characteristic plots of the powertrain operated with RBC control strategy for both cases are reported in Figure A2. The SoC trajectories (Figure A2a and Figure A2b) are subjected to a narrower range variation, with respect to what was observed with DP, however in the RBC emissions-oriented strategy the behavior for which the battery tends to be charged as soon as the driving cycle begins is conserved, as the ICE power is reduced (Figure A2d). Also, less energy can be provided through LPS operating mode. Moreover, Figure A2e and A2f show how effectively the ICE torque variation is controlled, with values below 80 Nm/s. This last feature gives more realistic values than those obtained in the DP optimization.

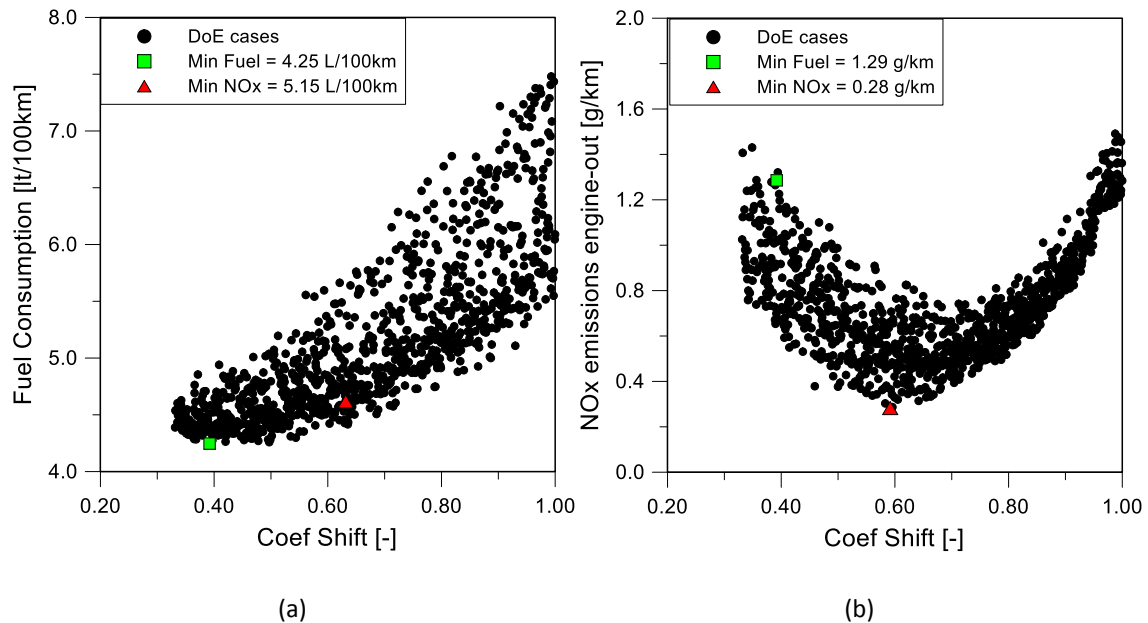


Figure 10 – Scatter plots of the DoE results: the best fuel-consumption-oriented and NOx emissions-oriented gearshift solutions are highlighted with a square and a triangle marker respectively

Table 7 shows the optimum parameters that provide the minimum fuel consumption (square marker) and minimum NOx emissions (triangle marker), shown in Figure 10. The emissions-oriented strategy uses the ICE in the low load region more than the fuel-economy-oriented strategy. To do that, the control strategy uses a lower

maximum EV speed mode and soft battery charging strategy (low $SoC_{@Power_{charge\ max}}$). This allows to turn on the ICE for a longer time and to maintain the battery with an energy content above the target, to help the ICE during the highway driving (last phase of the WLTC driving cycle). This avoids using the ICE in the high load region of the map, characterized by higher NOx emissions levels. Furthermore, the battery is used in a high range and so the power assist is lower in order to minimize the use of the ICE in high operative points to recharge the battery. It is important to note that for both optimum cases in the RBC, soot Euro 6 emissions limits are fulfilled (results are reported in Table 12) since with gearshift coefficients in the range of 0.33 and 0.66 (ICE speed between 1500 and 3000 rpm) both RCCI and CDC modes provide ultra-low soot emissions in the baseline dual mode combustion (Figure 3b).

Table 7 – Optimum calibration parameters for RBC in fuel economy and emissions-oriented strategies.

Hybrid Control Strategy	$Split_{coef}$	$v_{lim, EV}$	$Gearshift\ coefficient$	SoC_{charge}	$SoC_{@Power_{charge\ max}}$
RBC Fuel oriented	32%	115	0.39	0.40	0.55
RBC emissions oriented	6%	10	0.60	0.45	0.51

The a-ECMS calibration campaign was carried out by sweeping different values of gearshift coefficients and different values of NOx penalty β . The fuel economy-oriented strategy corresponds to $\beta = 0$. Each case was run with an iterative search method to determine the value of the constant term of the equivalence factor, s_0 , which allowed to have a null net battery energy balance at the end of the driving cycle. Hence, for a matter of computational cost reduction, the higher gearshift coefficient value explored was 0.66 (which corresponds to ICE speed upper boundary of RCCI region), above which no improvements were found in terms of both fuel consumption and NOx emissions abatement. For all cases, the SoC penalty factor k_p was kept equal to 1, as it was sufficient to contain the SoC trajectory within the desired SoC boundaries, and the SoC penalty exponential factor $q = 1$; the weight factor γ for the torque derivative penalty $p_2(\Delta T_{ICE}(t))$ was set to 1000, while the exponential term $t = 2$; NOx penalty exponential term $r = 1$. The results in terms of the total fuel consumption, total engine-out NOx are reported in Table 8 and 9, respectively. The calibration values for the constant term of the equivalence factor s_0 are reported in Table 10.

As can be inferred from Table 10, the calibration of a-ECMS main parameter, s_0 , becomes challenging at the borders of the RCCI region when the NOx penalty is set to high values. This can be clearly explained by the increasing difficulty with which the optimization phase fails to find the optimal control candidate.

The best configuration in terms of parameters setup can be selected from the previous results with a-ECMS. By looking at Table 8 and Table 9, the best a-ECMS fuel-economy-oriented strategy is selected for gearshift coefficient equals to 0.47 and for $s_0 = 2.8$ ($\beta = 0$), while the best a-ECMS emissions-oriented strategy is selected for

gearshift coefficient equals to 0.61, $s_0 = 6.2$ and $\beta = 5.0 * 10^7$. It is interesting to note that in both cases soot emissions Euro 6 limit is satisfied. The characteristic plots of the powertrain operated with a-ECMS control strategies are reported in Figure A3 of Appendix A. Figure A3a and A3b show that a-ECMS control strategy allows a greater variation of the battery SoC, compared to RBC control strategy. Also, the ICE power is reduced because of the effective control of its operation within the RCCI region for the emissions-oriented strategy compared to the fuel-economy one (Figure A3c and Figure A3d) while maintaining a good control of the ICE torque derivative (Figure A3e and A3f).

Table 8 – Fuel consumption results table for a-ECMS calibration with respect to different values of gearshift coefficient and NOx penalty weight factor β

<i>Fuel Consumption (L/100km)</i>							
	Gearshift Coefficient						
Beta	0.33	0.4	0.47	0.55	0.61	0.63	0.66
0	4.48	4.33	4.26	4.44	4.65	4.60	4.65
5.00E+05	4.41	4.44	4.53	4.62	4.67	4.74	4.81
5.00E+06	4.45	4.54	4.68	4.80	4.91	4.94	5.15
5.00E+07	4.44	4.57	4.71	4.82	4.96	4.97	5.47
5.00E+09	4.40	4.58	4.70	4.87	5.07	5.16	5.25
5.00E+10	/	4.58	4.70	4.91	5.24	5.86	5.24

Table 9 – Engine-out NOx emission results table for a-ECMS calibration with respect to different values of gearshift coefficient and NOx penalty weight factor β

<i>NOx emissions (g/km)</i>							
	Gearshift Coefficient						
Beta	0.33	0.4	0.47	0.55	0.61	0.63	0.66
0	1.26	1.19	0.88	0.68	0.44	0.51	0.44
5.00E+05	0.44	0.36	0.32	0.26	0.24	0.22	0.21
5.00E+06	0.25	0.20	0.16	0.13	0.13	0.12	0.17
5.00E+07	0.22	0.18	0.15	0.13	0.12	0.12	0.17
5.00E+09	0.23	0.18	0.16	0.13	0.13	0.14	0.15
5.00E+10	/	0.18	0.16	0.14	0.14	0.15	0.15

*Euro 6 NOx limits for CI is 0.080 g/km

Table 10 – a-ECMS equivalence factor constant term calibration with respect to different values of gearshift coefficient and NOx penalty weight factor β

Constant equivalence factor s_0							
	Gearshift Coefficient						
Beta	0.33	0.4	0.47	0.55	0.61	0.63	0.66
0	3.85	3.3	2.8	2.1	2.1	2.3	2.1
5.00E+05	12	8.5	5.8	4	3.3	3.3	3
5.00E+06	35	12	11	5.9	5.1	4.8	7.565
5.00E+07	140	18.9	13	6.4	6.2	6.2	30
5.00E+09	20000	19.1	17	10	10.5	55	1200
5.00E+10	/	19	19	12	231.485	1240	1200

Finally, online control strategies (RBC and a-ECMS) results are compared with the selected cases derived with DP in Table 11. The fuel consumption and emissions are also evaluated as relative percentage variation with respect to the baseline conventional CDC platform and the dual-mode RCCI-CDC platform. The a-ECMS and RBC fuel-consumption-oriented strategies show similar results in terms of fuel consumption, with a total reduction of 25% with respect to the conventional CDC no-hybrid vehicle. However, for the emissions-oriented case, a-ECMS strategy outperforms the RBC strategy and achieves lower NOx and soot emissions. This can be mainly explained by the improved capabilities of the control strategy to manage the power split between the ICE and EM. In fact, the calibration of the a-ECMS cost function parameters, s_0 and β , allows to use more proficiently the RCCI zone with respect to the RBC case.

In order to better understand the effect of the different control strategies on the ICE behavior, it is interesting to look at the ICE operating points on the NOx emissions map, as reported in Figure 11 (a discretization of 0.2 sis used). In terms of fuel economy oriented, the main target is to force the ICE to work in the higher load zone with low engine speed (below 1900 rpm). On the other hand, for the emissions-oriented case, it can be appreciated that the DP and a-ECMS provide better control to force the ICE to work in the RCCI region, than the RBC. This allows to achieve lower NOx emissions and better fuel consumption. The RBC is forced to operate in the lowest ICE load zone in which the brake thermal efficiency is low. In addition, it is interesting to note that the operating points in the RBC case are sparser and some fall outside the RCCI zone. Therefore, it is less efficient to operate in the RCCI region than the other two control strategies. Moreover, the time during which the ICE is actively used is greater with RBC than the DP and a-ECMS. This would result in an advantage for the last two mentioned strategies in terms of engine durability and wear. However, it can have a great impact in terms of engine exhaust temperature, hence on the efficiency of the ATS system. This is interesting for possible future works to understand the new developments required in terms of ATS design.

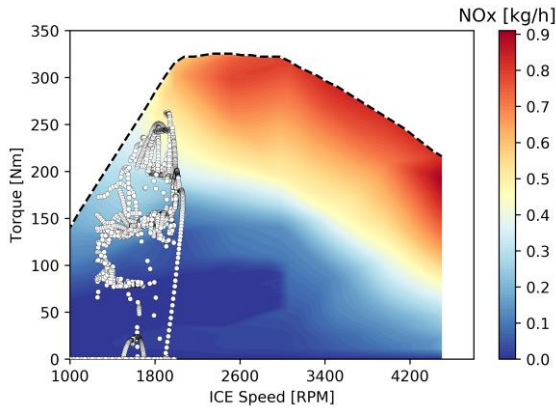
Table 11 - Results of the best calibration of control strategies, for fuel-oriented and emissions-oriented control strategies

Platform	Hybrid Control Strategy	Fuel Consumption	Relative Fuel Consumption difference	NOx Emissions	Relative NOx difference	Soot Emissions	Relative Soot difference
Unit	-	[L/100km]	[%]	[g/km]	[%]	[g/km]	[%]
No-hybrid CDC	-	5.65	-	0.480	-	0.0110	-
No-hybrid CDC + RCCI	-	5.73	+ 1	0.310	- 35	0.0040	- 64
P2-HEV CDC+RCCI	DP - FC	4.14	- 27	1.360	+ 183	0.0020	- 82
P2-HEV CDC + RCCI	DP - NOx	4.72	- 16	0.057	- 88	0.0006	- 94
P2 CDC + RCCI	RBC - FC	4.25	-25	1.290	+168	0.0027	- 75
P2 CDC + RCCI	RBC - NOx	5.15	- 9	0.280	- 42	0.0047	- 57
P2-HEV CDC + RCCI	aECMS - FC	4.26	- 25	0.880	+ 83	0.0030	- 73
P2-HEV CDC + RCCI	aECMS - NOx	4.96	- 12	0.120	- 75	0.0020	- 82

*Euro 6 NOx limits for CI is 0.080 g/km and Euro 6 Soot is 0.0050 g/km

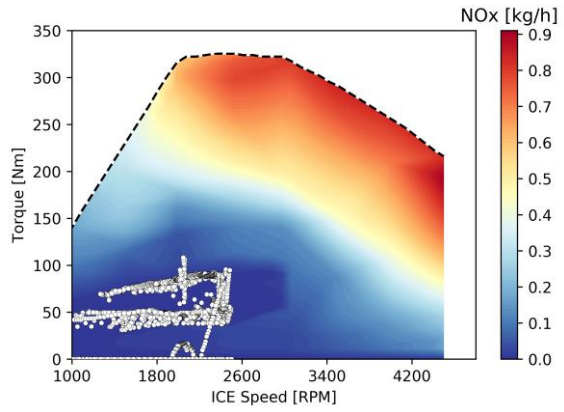
Dynamic Programming

Fuel Economy-oriented



(a)

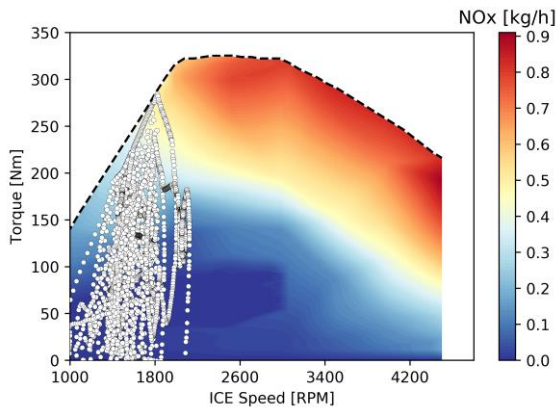
NOx emissions-oriented



(b)

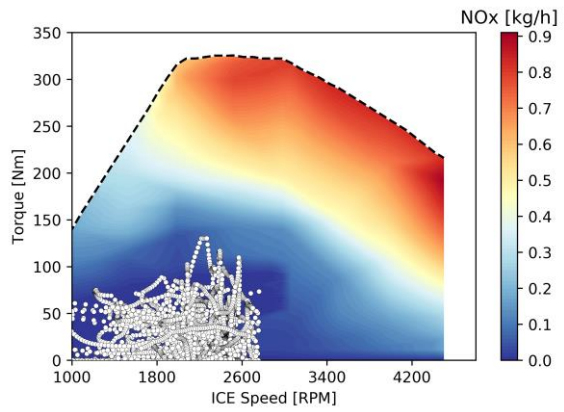
Rule Based Control strategy

Fuel Economy-oriented



(c)

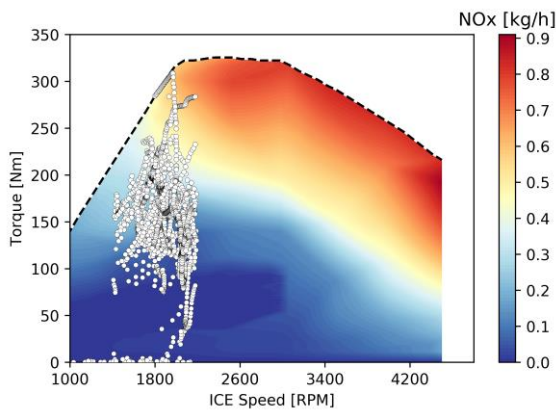
NOx emissions-oriented



(d)

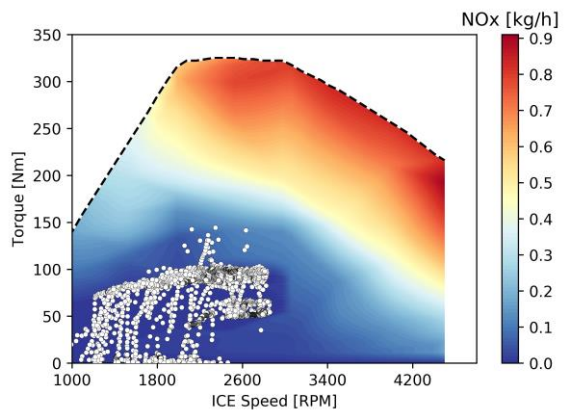
Adaptive Equivalent Consumption Minimization control Strategy

Fuel Economy-oriented



(e)

NOx emissions-oriented



(f)

Figure 11 – ICE NOx emission maps displaying the operative points of ICE for fuel-economy-oriented control strategies (left column) and emissions-oriented control strategies (right column)

4. Conclusions and future works

In this work it is investigated the potential of different on-line supervisory control strategies to operate a P2 parallel full hybrid electric vehicle equipped with an internal combustion engine running under dual-mode Reactivity Controlled Compression Ignition-Conventional Diesel combustion strategy. Two case scenarios were analyzed: a fuel-economy-oriented strategy and a nitrogen-oxides-emissions-oriented strategy.

- A preliminary design procedure, based on dynamic programming, was adopted to determine the best sizes of the battery capacity and electric machine power to evaluate each control strategy.
- The design of experiment analysis allows to found that the battery capacity and electric machine power must be 6.9 Ah and 20 kW respectively, to achieve the minimum fuel consumption (4.72 L/100km) while fulfilling the Euro 6 NOx emissions (0.057 g/km). This configuration was used as input to size the vehicle electric grid in the Gt-Suite model, where the online control strategies of Rule-Based Control and Adaptive Equivalent Consumption Minimization Strategy were tested.
- The comparison of the two control strategies showed that the latter, apart from the benefits it has in terms of calibration with respect to the former, enables a more successful control to operate the engine towards the medium-low loads region where Reactivity Controlled Compression Ignition combustion is actuated.
- This results in a 30% reduction of both nitrogen oxides emissions and soot emissions with respect to the RBC emissions-oriented strategy.
- Furthermore, the benefits of lower engine-out emissions, thanks to the integration of RCCI combustion in a hybrid powertrain, demonstrate how this technology can enable successful use of diesel engines to meet upcoming regulations, also considering the potential downsizing of the aftertreatment system that could lower the total powertrain costs.

Despite the Adaptive Equivalent Consumption Minimization Strategy allows a reduction of nitrogen oxides emissions of 75% with respect to the baseline conventional diesel combustion emissions, it was not enough to achieve the Euro 6 legislation as it was obtained in the case of dynamic programming control strategy. Hence, this suggests that there is space for future improvements on the supervisory energy management control strategy for the P2 parallel full hybrid electric vehicle, for instance by adopting predictive capabilities such as driving cycle prediction or driving pattern recognition, among others. Additionally, the present study could be extended also by looking at two aspects: the first concerns a thorough analysis of the influence of ICE transient control to switch between the two combustion modes (Reactivity Controlled Compression Ignition and Conventional Diesel combustion modes) on the engine-out emissions; the second one regards the influence of the battery thermal management on the discussed energy management strategies, in fact the two on-line control strategies make a different use of the battery energy content, resulting in different battery state of charge trajectories over the World-wide harmonized Light-duty Test Cycle. This could lead to

an interesting analysis regarding battery aging, which is another important aspect concerning hybrid electric vehicles that must be controlled to ensure a successful powertrain design.

Declaration of Interests

The authors declare no conflict of interest.

Acknowledgments

The authors acknowledge FEDER and Spanish Ministerio de Economía y Competitividad for partially supporting this research through TRANCO project (TRA2017-87694-R). The authors also acknowledge the Universitat Politècnica de València for partially supporting this research through Convocatoria de ayudas a Primeros Proyectos de Investigación (SP20180148).

Abbreviations

ATS – After-Treatment System

BTE – Break Thermal Efficiency

CDC – Conventional Diesel Combustion

CO – Carbon Monoxide

CO₂ – Carbon Dioxide

DI – Direct Injection

DOC – Diesel Oxidation Catalyst

DP – Dynamic Programming

ECMS – Equivalent Consumption Minimization Strategy

ECU – Engine Control Unit

EGR – Exhaust Gas Recirculation

EM – Electric Machine

FHEV – Full Hybrid Electric Vehicle

GF – Gasoline Fraction

GM – General Motors

ICE – Internal Combustion Engine

LPS – Load Point Shifting

LTC – Low Temperature Combustion

MPPR – Maximum Pressure Rise Rate

NEDC – New European Driving Cycle

NOx - Oxides of Nitrogen

OEM – Original Equipment Manufacturer

PFI – Port Fuel Injection

PRR – Pressure Rise Rate

RCCI – Reactivity Controlled Compression Ignition

RDE – Real Driving Emission cycle

RBC – Rule-Based Control strategy

REESS – Rechargeable Electric Energy Storage System

SoC – State of Charge

THC – Total Hydrocarbons

WLTC – World-wide harmonized Light-duty Test Cycle

References

- [1] European Commission. REGULATION (EU) 2019/631 OF THE EUROPEAN PARLIAMENT AND OF THE COUNCIL of 17 April 2019 setting CO₂ emission performance standards for new passenger cars and for new light commercial vehicles, and repealing Regulations (EC) No 443/2009 and (EU) No 510/2011. Off J Eur Union 2019;25.4.2019.
- [2] European Parliament, Council of the European Union. REGULATION (EC) No 715/2007 OF THE EUROPEAN PARLIAMENT AND OF THE COUNCIL of 20 June 2007 on type approval of motor vehicles with respect to emissions from light passenger and commercial vehicles (Euro 5 and Euro 6) and on access to vehicle repair and maintenance. Off J Eur Union 2007;L171:1–16. <https://doi.org/OJEU.2007.L171>.
- [3] Palmer K, Tate JE, Wadud Z, Nellthorp J. Total cost of ownership and market share for hybrid and electric vehicles in the UK, US and Japan. Appl Energy 2018;209:108–19. <https://doi.org/10.1016/j.apenergy.2017.10.089>.
- [4] Wu Z, Wang C, Wolfram P, Zhang Y, Sun X, Hertwich E. Assessing electric vehicle policy with region-specific carbon footprints. Appl Energy 2019;256:113923. <https://doi.org/10.1016/j.apenergy.2019.113923>.
- [5] Hofmann J, Guan D, Chalvatzis K, Huo H. Assessment of electrical vehicles as a successful driver for reducing CO₂ emissions in China. Appl Energy 2016;184:995–1003. <https://doi.org/10.1016/j.apenergy.2016.06.042>.
- [6] Senecal PK, Leach F. Diversity in transportation: Why a mix of propulsion technologies is the way forward for the future fleet. Results Eng 2019;4:100060. <https://doi.org/10.1016/j.rineng.2019.100060>.

- [7] Benajes J, García A, Monsalve-Serrano J, Balloul I, Pradel G. An assessment of the dual-mode reactivity controlled compression ignition/conventional diesel combustion capabilities in a EURO VI medium-duty diesel engine fueled with an intermediate ethanol-gasoline blend and biodiesel. *Energy Convers Manag* 2016;123:381–91. <https://doi.org/10.1016/j.enconman.2016.06.059>.
- [8] Benajes J, García A, Monsalve-Serrano J, Balloul I, Pradel G. Evaluating the reactivity controlled compression ignition operating range limits in a high-compression ratio medium-duty diesel engine fueled with biodiesel and ethanol. *Int J Engine Res* 2017;18:66–80. <https://doi.org/10.1177/1468087416678500>.
- [9] Benajes J, García A, Monsalve-Serrano J, Villalta D. Benefits of E85 versus gasoline as low reactivity fuel for an automotive diesel engine operating in reactivity controlled compression ignition combustion mode. *Energy Convers Manag* 2018;159:85–95. <https://doi.org/10.1016/j.enconman.2018.01.015>.
- [10] Benajes J, García A, Monsalve-serrano J, Sari RL. Experimental investigation on the efficiency of a diesel oxidation catalyst in a medium-duty multi-cylinder RCCI engine. *Energy Convers Manag* 2018;176:1–10. <https://doi.org/10.1016/j.enconman.2018.09.016>.
- [11] García A, Piqueras P, Monsalve-serrano J, Sari RL. Sizing a conventional diesel oxidation catalyst to be used for RCCI combustion under real driving conditions. *Appl Therm Eng* 2018;140:62–72. <https://doi.org/10.1016/j.applthermaleng.2018.05.043>.
- [12] García A, Monsalve-Serrano J. Analysis of a series hybrid vehicle concept that combines low temperature combustion and biofuels as power source. *Results Eng* 2019;1:100001. <https://doi.org/10.1016/j.rineng.2019.01.001>.
- [13] Benajes J, García A, Monsalve-Serrano J, Sari R. Potential of RCCI series hybrid vehicle architecture to meet the future CO₂ targets with low engine-out emissions. *Appl Sci* 2018;8:1472. <https://doi.org/10.3390/app8091472>.
- [14] Zhuang W, Li (Eben) S, Zhang X, Kum D, Song Z, Yin G, et al. A survey of powertrain configuration studies on hybrid electric vehicles. *Appl Energy* 2020;262:114553. <https://doi.org/10.1016/j.apenergy.2020.114553>.
- [15] Benajes J, García A, Monsalve-serrano J, Martínez-boggio S. Optimization of the parallel and mild hybrid vehicle platforms operating under conventional and advanced combustion modes. *Energy Convers Manag* 2019;190:73–90. <https://doi.org/10.1016/j.enconman.2019.04.010>.
- [16] Shabbir W, Evangelou SA. Threshold-changing control strategy for series hybrid electric vehicles. *Appl Energy* 2019;235:761–75. <https://doi.org/10.1016/j.apenergy.2018.11.003>.
- [17] Paganelli G. General supervisory control policy for the energy optimization of charge-sustaining hybrid electric vehicles. *JSAE Rev* 2001;22:511–8. [https://doi.org/10.1016/s0389-4304\(01\)00138-2](https://doi.org/10.1016/s0389-4304(01)00138-2).
- [18] Lei Z, Qin D, Hou L, Peng J, Liu Y, Chen Z. An adaptive equivalent consumption

minimization strategy for plug-in hybrid electric vehicles based on traffic information. *Energy* 2020;190:116409.
<https://doi.org/10.1016/j.energy.2019.116409>.

- [19] Li Y, Jiao X. Energy management strategy for hybrid electric vehicles based on adaptive equivalent consumption minimization strategy and mode switching with variable thresholds. *Sci Prog* 2020;103:36850419874992.
<https://doi.org/10.1177/0036850419874992>.
- [20] Zhang Y, Chu L, Fu Z, Guo C, Zhao D, Li Y, et al. An improved adaptive equivalent consumption minimization strategy for parallel plug-in hybrid electric vehicle. *Proc Inst Mech Eng Part D J Automob Eng* 2019;233:1649–63.
<https://doi.org/10.1177/0954407018805605>.
- [21] Stroe N, Olaru S, Colin G, Ben-Cherif K, Chamaillard Y. A two-layer predictive control for hybrid electric vehicles energy management. *IFAC-PapersOnLine* 2017;50:10058–64. <https://doi.org/10.1016/j.ifacol.2017.08.1777>.
- [22] Wang Y, Wang X, Sun Y, You S. Model predictive control strategy for energy optimization of series-parallel hybrid electric vehicle. *J Clean Prod* 2018;199:348–58. <https://doi.org/10.1016/j.jclepro.2018.07.191>.
- [23] Zhou Y, Ravey A, Péra MC. Multi-mode predictive energy management for fuel cell hybrid electric vehicles using Markov driving pattern recognizer. *Appl Energy* 2020;258:114057. <https://doi.org/10.1016/j.apenergy.2019.114057>.
- [24] Finesso R, Spessa E, Venditti M. Layout design and energetic analysis of a complex diesel parallel hybrid electric vehicle. *Appl Energy* 2014;134:573–88.
<https://doi.org/10.1016/j.apenergy.2014.08.007>.
- [25] Qin Z, Luo Y, Zhuang W, Pan Z, Li K, Peng H. Simultaneous optimization of topology, control and size for multi-mode hybrid tracked vehicles. *Appl Energy* 2018;212:1627–41. <https://doi.org/10.1016/j.apenergy.2017.12.081>.
- [26] He Y, Wang C, Zhou Q, Li J, Makridis M, Williams H, et al. Multiobjective component sizing of a hybrid ethanol-electric vehicle propulsion system. *Appl Energy* 2020;266. <https://doi.org/10.1016/j.apenergy.2020.114843>.
- [27] Finesso R, Spessa E, Venditti M. Cost-optimized design of a dual-mode diesel parallel hybrid electric vehicle for several driving missions and market scenarios. *Appl Energy* 2016;177:366–83. <https://doi.org/10.1016/j.apenergy.2016.05.080>.
- [28] Musardo C, Staccia B, Midlam-Mohler S, Guezennec Y, Rizzoni G. Supervisory control for NOx reduction of an HEV with a mixed-mode HCCI/CIDI engine. *Proc Am Control Conf* 2005;6:3877–81. <https://doi.org/10.1109/acc.2005.1470579>.
- [29] Nüesch T, Cerofolini A, Mancini G, Cavina N, Onder C, Guzzella L. Equivalent Consumption Minimization Strategy for the Control of Real Driving NOx Emissions of a Diesel Hybrid Electric Vehicle. *Energies* 2014;7:3148–78.
<https://doi.org/10.3390/en7053148>.
- [30] Benajes J, García A, Monsalve-serrano J, Villalta D. Exploring the limits of the reactivity controlled compression ignition combustion concept in a light-duty

- diesel engine and the influence of the direct-injected fuel properties. *Energy Convers Manag* 2018;157:277–87.
<https://doi.org/10.1016/j.enconman.2017.12.028>.
- [31] Benajes J, García A, Monsalve-Serrano J, Boronat V. Gaseous emissions and particle size distribution of dual-mode dual-fuel diesel-gasoline concept from low to full load. *Appl Therm Eng* 2017;120:138–49.
<https://doi.org/10.1016/j.applthermaleng.2017.04.005>.
- [32] Winke F. Transient Effects in Simulations of Hybrid Electric Drivetrains. 2019.
<https://doi.org/10.1007/978-3-658-22554-4>.
- [33] Luján JM, García A, Monsalve-Serrano J, Martínez-Boggio S. Effectiveness of hybrid powertrains to reduce the fuel consumption and NOx emissions of a Euro 6d-temp diesel engine under real-life driving conditions. *Energy Convers Manag* 2019;199:111987. <https://doi.org/10.1016/j.enconman.2019.111987>.
- [34] Petersheim MD, Brennan SN. Scaling of hybrid-electric vehicle powertrain components for Hardware-in-the-loop simulation. *Mechatronics* 2009;19:1078–90. <https://doi.org/10.1016/j.mechatronics.2009.08.001>.
- [35] Emadi A. Handbook of automotive power electronics and motor drives. 2017.
<https://doi.org/10.1201/9781420028157>.
- [36] A123 Systems. Nanophosphate High Power Lithium Ion Cell ANR26650 m1-B 316AD:400. <https://www.batteryspace.com/prod-specs/6610.pdf> (accessed March 27, 2020).
- [37] Perez HE, Siegel JB, Lin X, Stefanopoulou AG, Ding Y, Castanier MP. Parameterization and Validation of an Integrated Electro-Thermal Cylindrical LFP Battery Model. Vol. 3 *Renew. Energy Syst. Robot. Robust Control. Single Track Veh. Dyn. Control. Stoch. Model. Control Algorithms Robot. Struct. Dyn. Smart Struct.*, vol. 3, ASME; 2012, p. 41–50. <https://doi.org/10.1115/DSCC2012-MOVIC2012-8782>.
- [38] Feng X, Ouyang M, Liu X, Lu L, Xia Y, He X. Thermal runaway mechanism of lithium ion battery for electric vehicles: A review. *Energy Storage Mater* 2018;10:246–67. <https://doi.org/10.1016/j.ensm.2017.05.013>.
- [39] Bayar K, Biasini R, Onori S, Rizzoni G. Modelling and control of a brake system for an extended range electric vehicle equipped with axle motors. *Int J Veh Des* 2012;58:399–426. <https://doi.org/10.1504/IJVD.2012.047387>.
- [40] Nations U. Addendum 12: Regulation No. 13 2011.
- [41] Sundstrom O, Guzzella L. A generic dynamic programming Matlab function. 2009 IEEE Int. Conf. Control Appl., IEEE; 2009, p. 1625–30.
<https://doi.org/10.1109/CCA.2009.5281131>.
- [42] Onori S, Serrao L. On Adaptive-ECMS strategies for hybrid electric vehicles. *Les Rencontres Sci d'IFP Energies Nouv* 2011:1–7.
- [43] Serrao L, Onori S, Rizzoni G. A comparative analysis of energy management

strategies for hybrid electric vehicles. *J Dyn Syst Meas Control Trans ASME* 2011;133. <https://doi.org/10.1115/1.4003267>.

- [44] Grondin O, Thibault L, Quérel C. Lois de gestion de l'énergie pour le véhicule hybride Diesel. *Oil Gas Sci Technol* 2015;70:125–41. <https://doi.org/10.2516/ogst/2013215>.

Appendix A

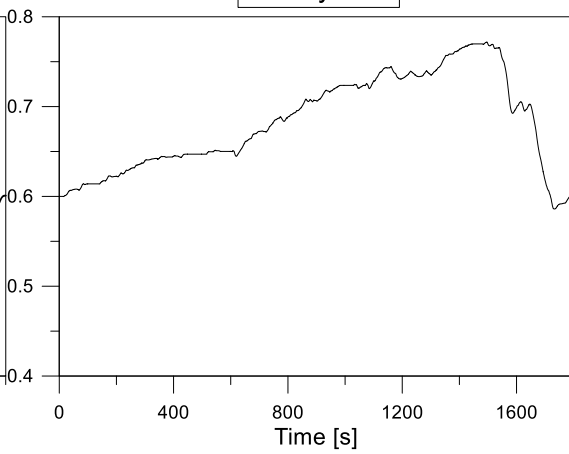
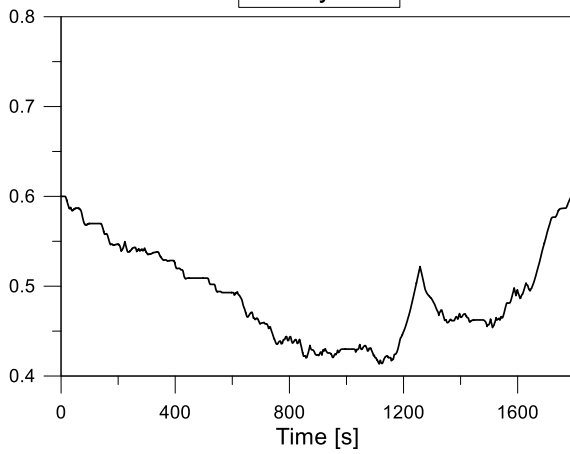
Figure A1, A2 and A3 show the results of the P2 parallel full-hybrid powertrain over a WLTC driving cycle, when operated respectively with DP, RBC and a-ECMS control strategies. In all these figures, the left column refers to the fuel-economy oriented calibration, while the right column refers to the NOx emissions-oriented calibration. In this way, the difference between the two calibrations in terms of energy management can be appreciated. SoC trajectory, ICE and EM torque outputs, first time derivative of ICE torque output and operating points of EM are represented. Plots of ICE operating points are presented in Figure 11 in the manuscript main body. On-line supervisory energy management control strategies based on RBC and a-ECMS are calibrated so to ensure a maximum deviation of the final battery SoC to the SoC target (equal to 0.6) of $\pm 1\%$ in order to enable a fair comparison between the strategies. The general observation can be drawn: in the NOx emissions-oriented strategy case, as the ICE output power is limited to operate in the RCCI region of the engine map, the supervisory energy management control makes the ICE to operate at an almost constant regime, right from the beginning of the driving cycle, with the objective to store enough energy in the battery that is later used in the highway section of the WLTC driving cycle, where the energy demand is higher. It must be furthermore noted the effort to control the ICE dynamic behavior by limiting the torque time derivative within the prescribed limits.

Fuel-Economy-oriented DOE optimization

NOx emissions-oriented DOE optimization

Battery SoC

Battery SoC

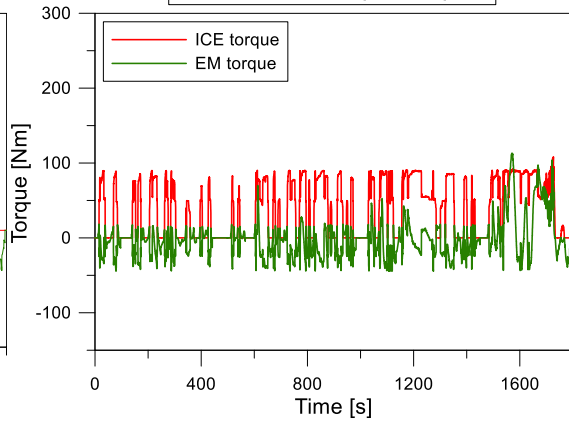
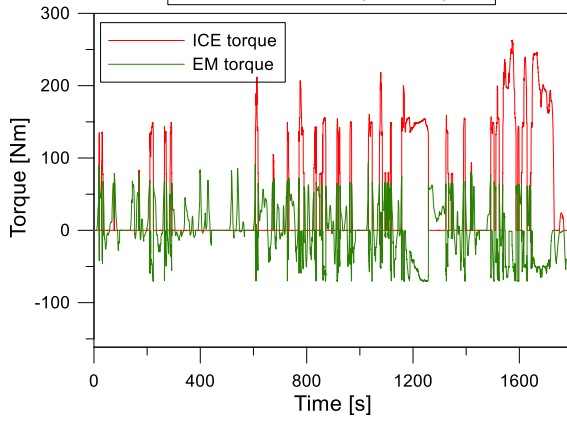


(a)

(b)

ICE and EM torque outputs

ICE and EM torque outputs

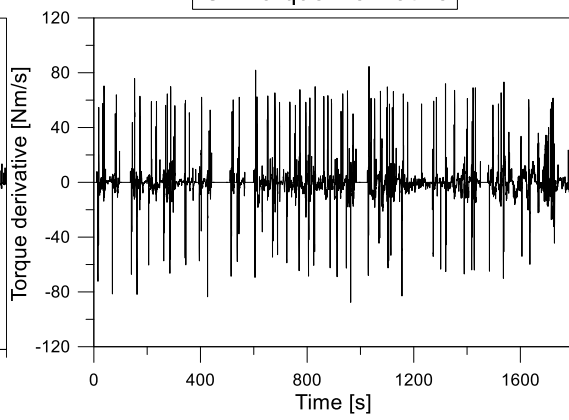
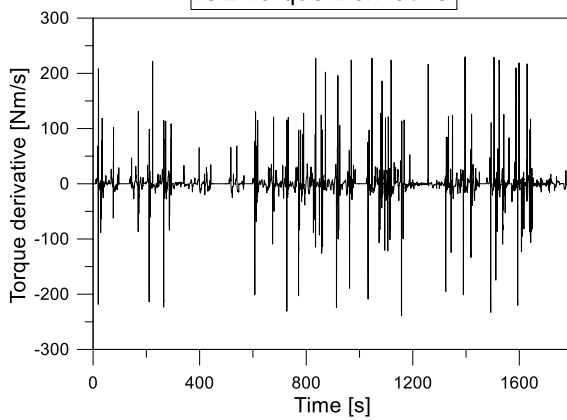


(c)

(d)

ICE Torque Derivative

ICE Torque Derivative



(e)

(f)

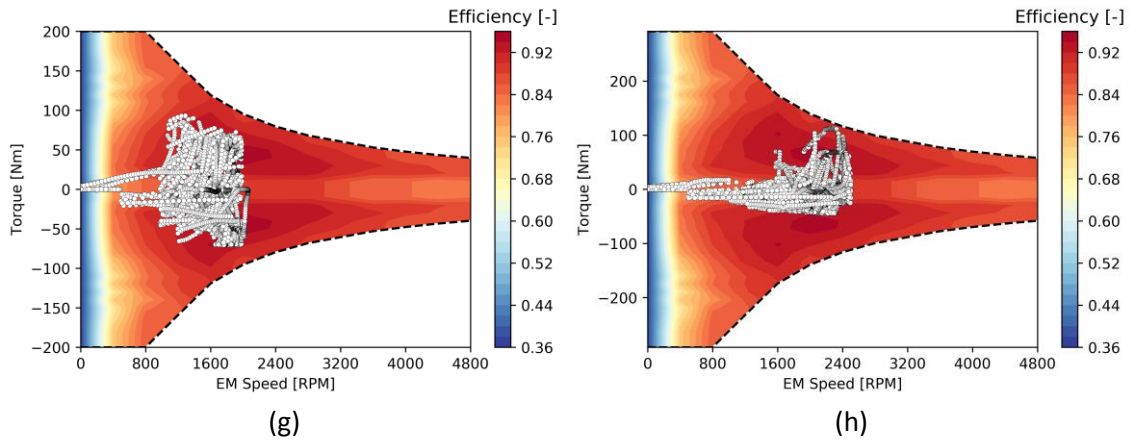
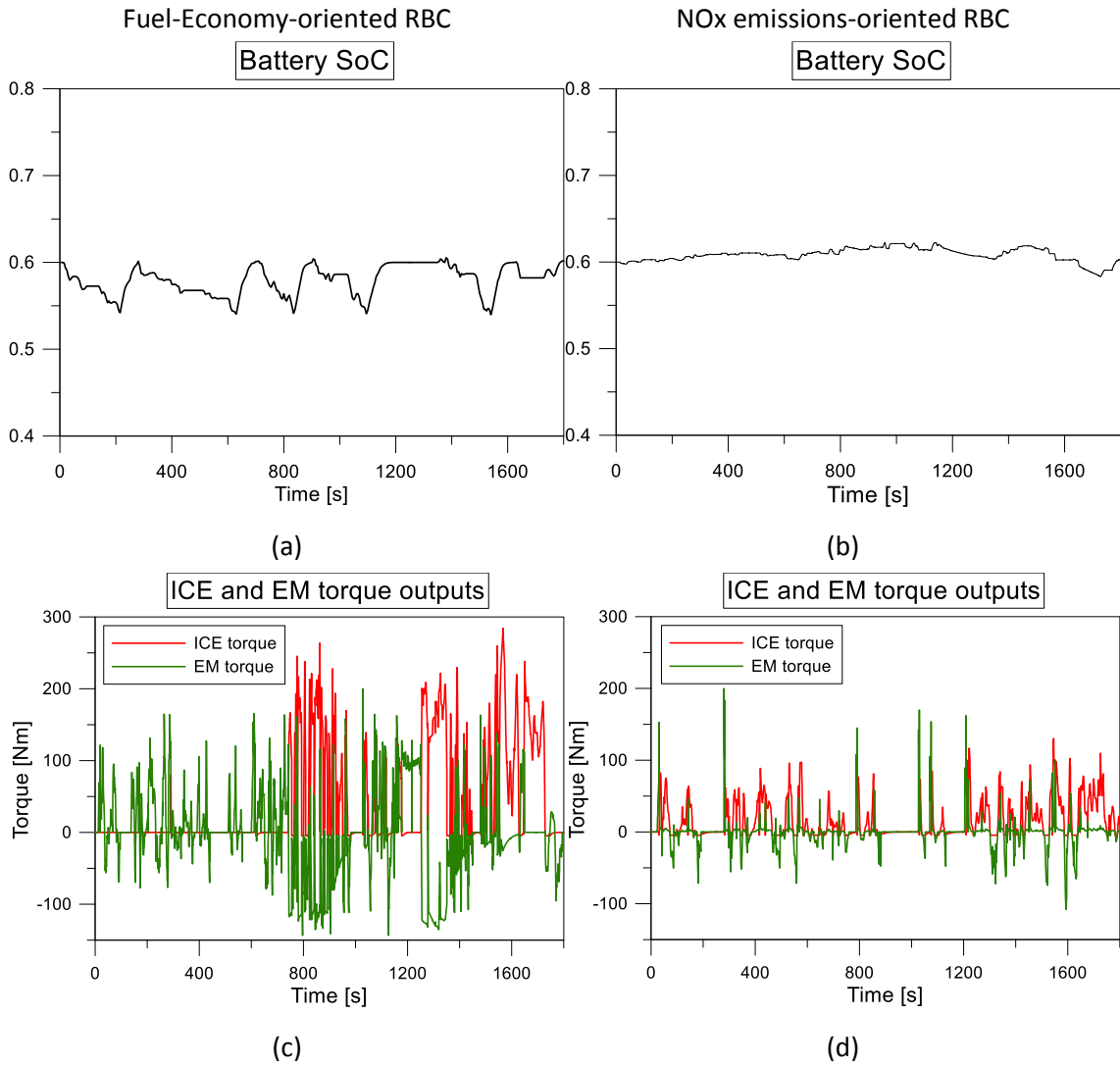


Figure A1 – Characteristic plots of the best configurations obtained with the preliminary design analysis performed with Dynamic Programming. Left column: fuel-economy-oriented optimization (Battery capacity = 6.9 Ah, EM power = 20 kW). Right column: emissions-oriented optimization (Battery capacity = 9.2 Ah, EM power = 36.5 kW)



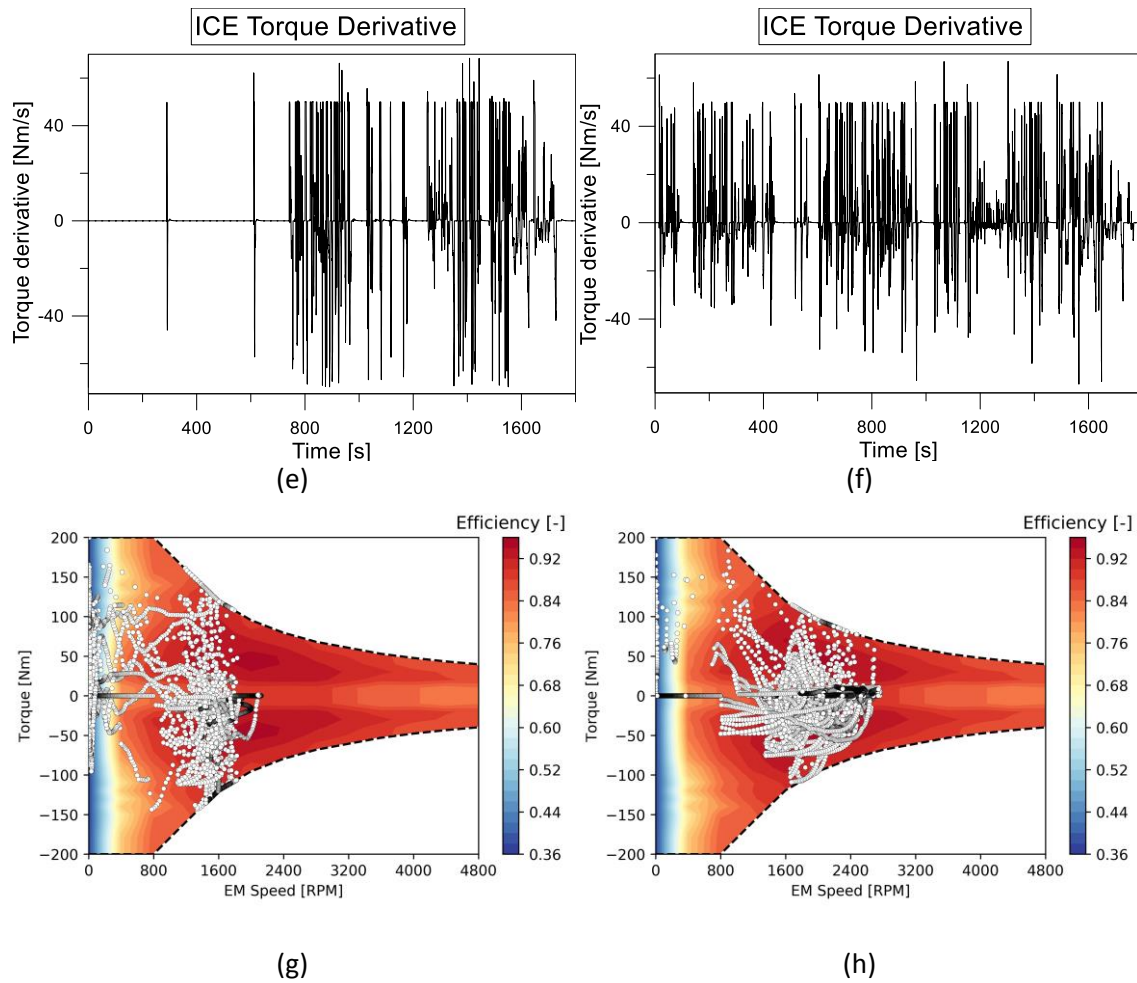
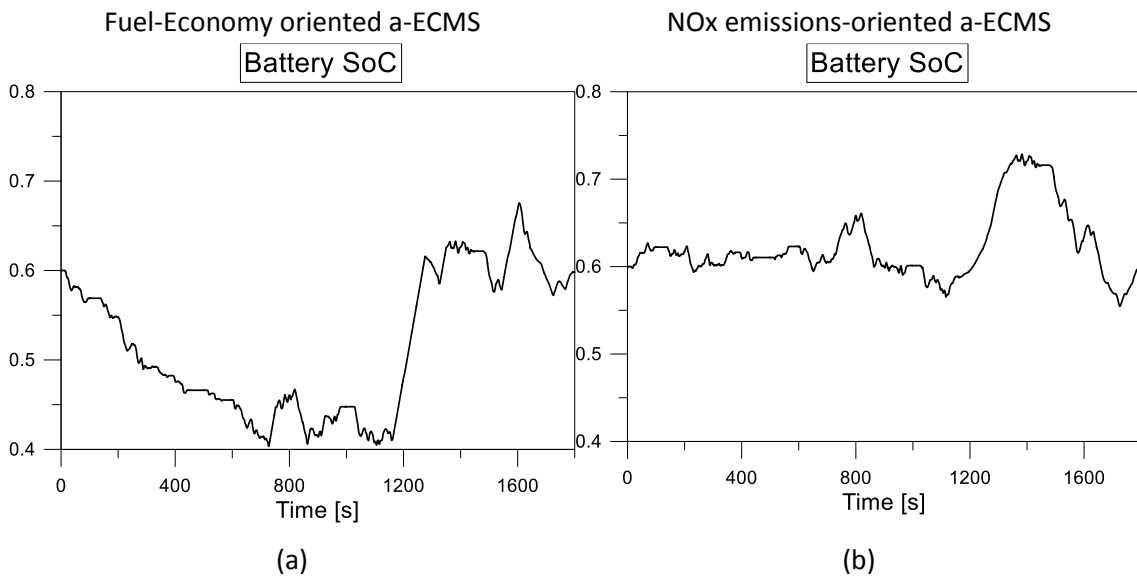


Figure A2 – Characteristic plots of optimal calibration for RBC fuel-economy-oriented strategy (left column) and RBC emissions-oriented strategy (right column)



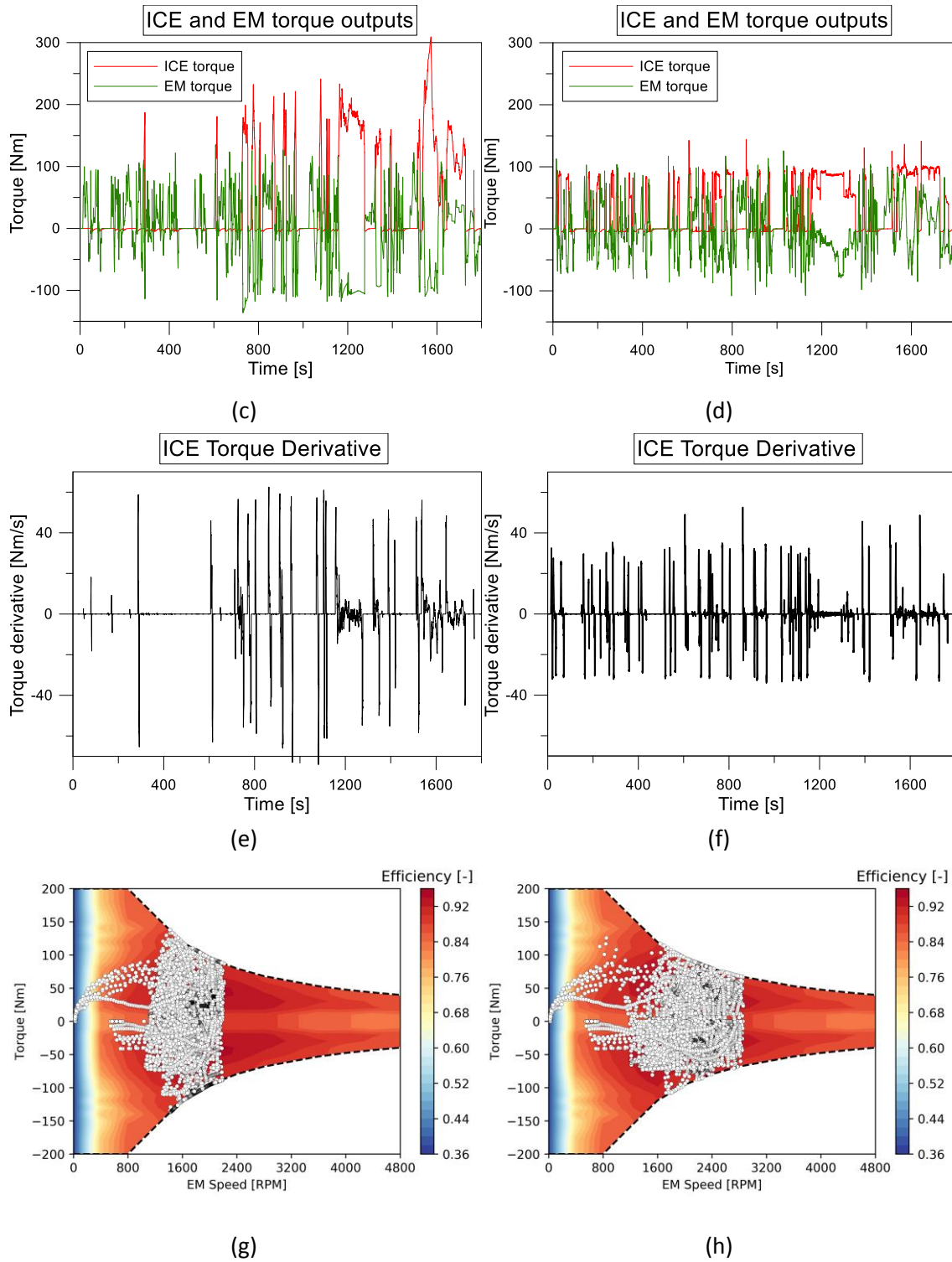


Figure A3 - Characteristic plots of optimal calibration for a-ECMS fuel-economy-oriented strategy (left column) and a-ECMS emissions-oriented strategy (right column)